CANCER

Interdomain spacing and spatial configuration drive the potency of IgG-[L]-scFv T cell bispecific antibodies

Brian H. Santich[1,2], Jeong A. Park[2], Hoa Tran[2], Hong-Fen Guo[2], Morgan Huse[3], Nai-Kong V. Cheung[2]*

T cell–bispecific antibodies (BsAbs) couple cytotoxic T lymphocytes to tumor cells, inducing their destruction. Although there are more than 60 classes of BsAbs in development, the relative importance of parameters such as interdomain spacing or spatial configuration is largely unknown. Here, we dissected a symmetric dual bivalent BsAb platform (IgG-[L]-scFv: antitumor IgG with anti-CD3 scFv fused to the light chains) to explore the importance of valency and spatial configuration for BsAb-induced T cell cytotoxicity. Our results revealed that placing tumor and T cell binding domains on the same side of a BsAb (cis-configuration) elicited substantially stronger antitumor activity, in vitro and in vivo, compared to positioning them on opposite sides (trans-configuration). Moreover, using two cis-modules in the same BsAb further improved cytotoxicity (up to 2000-fold). In addition, separating antigen-binding components with a single Ig domain (C_L) markedly enhanced cytokine release and in vivo tumor responses compared to smaller (G_4S_1) or larger (C_{H1}-C_{H2}-C_{H3}) spacers. These findings provide guidelines for improving BsAb function and highlight the importance of spatial configuration and dual bivalency as development parameters.

INTRODUCTION

In recent years, bispecific antibody (BsAb) development has emerged as a promising strategy for the treatment of clotting deficiency (*1*) and cancer (*2*–*4*). Although only two different formats have been used in U.S. Food and Drug Administration (FDA)–approved BsAbs to date (*1*, *2*), there are more than 60 currently in preclinical and clinical development (*5*–*7*). This proliferation of different BsAb formats has generated a panoply of designs with distinct sizes, valencies, and interdomain configurations. Although studies have suggested that molecular size and tumor binding affinity can influence biodistribution (*8*) and cytotoxicity (*9*), respectively, the importance of other structural features remains largely unknown. Systematic efforts to identify the parameters that most influence in vitro and in vivo BsAb potency are critical for developing the best therapeutics to improve outcomes in the clinic.

We have previously described several highly potent T cell–engaging BsAbs using the symmetric and dual bivalent IgG–[L]-scFv platform (*10*–*13*), in which a single-chain variable fragment (scFv) recognizing human CD3ε (huCD3ε) is fused to the C termini of each antitumor Immunoglobulin G (IgG) antibody light chain (Fig. 1A). Although this design has consistently provided exceptionally strong in vitro and in vivo antitumor activity against multiple tumor antigens [ganglioside GD2 (*13*), CD33 (*10*), GPA33 (*11*), and HER2 (*12*)], the basis for its efficacy is poorly understood.

In the present study, we examined a particularly powerful GD2-specific IgG-[L]-scFv reagent and identified architectural features that explain its robust antitumor activity. First, we confirmed the importance of valency for improving in vitro cytotoxicity. Next, we demonstrated that separation of tumor and T cell binding domains using a single Ig domain (C_L) drastically improved in vitro cytokine secretion and in vivo antitumor responses compared to smaller (G_4S_1) or larger (C_{H1}-C_{H2}-C_{H3}) spacers. Last, through systematic reengineering of the IgG-[L]-scFv design, we showed that placing tumor and T cell binding domains on the same side of a BsAb (cis-configuration) improved cytotoxic potencies 50-fold and that uniting two such cis-modules together in one dual bivalent format increased in vitro cytotoxicity an additional 30-fold, markedly enhancing naïve T cell responses both in vitro and in vivo. Hence, the potency of a BsAb results not only from its valency but also from the spacing and spatial configuration of its antigen-binding domains.

RESULTS

IgG-[L]-scFv format is substantially more potent than other common BsAb designs

We began our study by comparing the IgG-[L]-scFv format to two BsAb formats widely used for T cell redirection applications: the bispecific T cell engager (BiTE; same format as the FDA-approved blinatumomab) and the IgG heterodimer (Fig. 1A and table S1). Each BsAb was engineered to recognize ganglioside GD2 (GD2) on tumor cells and huCD3ε on T cells using the variable domain sequences of humanized 3F8 (hu3F8) (*14*) and humanized OKT3 (huOKT3) (*15*), respectively. Both the BiTE and the IgG-[L]-scFv BsAbs were produced using standard mammalian expression and affinity purification, whereas the IgG heterodimer was made through the controlled Fab-arm exchange (*16*) of two distinct IgG homodimers (hu3F8 IgG and huOKT3 IgG). For each of these parental IgG molecules, one of two Fc mutations was introduced (hu3F8 with K409R or huOKT3 with F405L) to facilitate their monomerization and preferential heterodimerization under reducing conditions (Fig. 1B and table S1).

We measured the binding kinetics of each BsAb format against GD2 and huCD3ε using surface plasmon resonance (SPR) (tables S2 and S3). Expectedly, the IgG-[L]-scFv, hereafter called 2+2 (for two anti-GD2 and two anti-huCD3ε domains), displayed higher apparent affinity for both antigens (3 nM equilibrium dissociation constant (K_D) for GD2 and 6 nM for huCD3ε) when compared to both the BiTE (11 nM K_D for GD2 and 13 nM for huCD3ε) and IgG heterodimer (15 nM K_D for GD2 and 130 nM for huCD3ε), hereafter called 1+1B and 1+1H (for one anti-GD2 and anti-huCD3ε domain),

[1]Louis V. Gerstner Jr. Graduate School of Biomedical Sciences, Memorial Sloan Kettering Cancer Center, New York, NY 10065, USA. [2]Department of Pediatrics, Memorial Sloan Kettering Cancer Center, New York, NY 10065, USA. [3]Immunology Program, Memorial Sloan Kettering Cancer Center, New York, NY 10065, USA.
*Corresponding author. Email: cheungn@mskcc.org

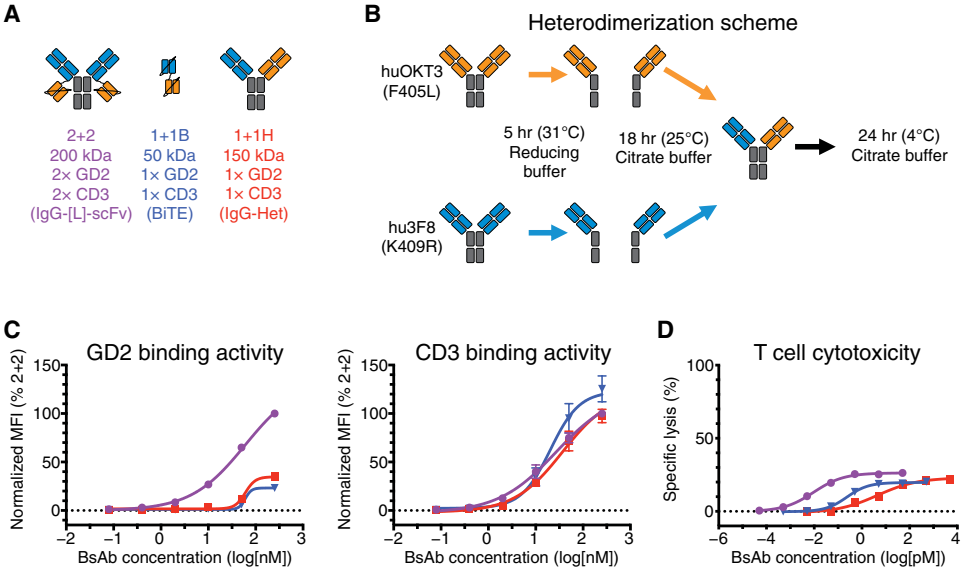

Fig. 1. In vitro comparison of IgG-[L]-scFv to common BsAb designs. (**A**) Schematic of BsAb panel: IgG-[L]-scFv (2+2), BiTE (1+1B), and IgG heterodimer (1+1H). Orange domains represent anti-huCD3ε domains (derived from huOKT3), and blue domains represent anti-GD2 domains (derived from hu3F8). (**B**) Schematic of the IgG heterodimerization by controlled Fab arm exchange. (**C**) Representative cell-binding activity of each BsAb against GD2$^+$ human M14 melanoma cells (left) and CD3$^+$ huATCs (right), measured by flow cytometry. Geometric mean fluorescence intensity (MFI) was normalized to 2+2 (100%) for each BsAb. (**D**) Representative T cell–dependent cytotoxicity for each BsAb. For reference: 2+2 is purple, 1+1B is blue, and 1+1H is red. Each curve represents one BsAb, and each point represents a single concentration, with two (flow cytometry) or three (cytotoxicity) technical replicates. Data are shown as means ± SD.

respectively. Binding to antigen-expressing cells was evaluated by flow cytometry (Fig. 1C and data file S1), detecting bound BsAbs with anti-idiotypic antibodies that recognized either the anti-huCD3ε domains (to measure GD2 binding) or the anti-GD2 domains (to measure CD3 binding) of each BsAb. Here, 2+2 bound GD2$^+$ human M14 melanoma cells much more effectively than 1+1H or 1+1B, both in terms of maximum and half-maximal effective concentration (EC_{50}), whereas all three formats bound similarly to activated human T cells (huATCs).

To assess the potency of each format, we performed in vitro cytotoxicity assays where the BsAbs engaged huATCs against M14 human melanoma cells (Fig. 1D and table S1). 2+2 (9 fM EC_{50}) was more than 500-fold more potent than 1+1H (4 pM EC_{50}) and more than 20-fold more potent than 1+1B (230 fM EC_{50}). To confirm that these differences were not specific to the hu3F8 sequence, two additional anti-GD2 sequences (GD2.2 and GD2.3) were used to build both 2+2 and 1+1H formats (table S4). Both constructs recapitulated the in vitro cytotoxicity differences seen with the hu3F8-based 2+2 and 1+1H formats (857- and 1959-fold, respectively), suggesting that the markedly enhanced potency of 2+2 was not unique to the hu3F8 sequence. These results were also consistent with prior studies showing that a 2+2 BsAb directed against CD33 was 100-fold more cytotoxic than its 1+1H counterpart (*10*), indicating that this major difference in cytotoxicity was not restricted to GD2 or membrane-proximal antigens. We also prepared 1+1B-formatted BsAb using the GD2.2 and GD2.3 sequences. Although only one of these (GD2.2) could express at high enough purity (>80% monomer) to make meaningful interpretations, it too showed reduced potency compared to the analogous 2+2 (table S4). Last, to determine whether the enhanced efficacy of 2+2 resulted from unique properties of the huOKT3 sequence or epitope, we made 2+2 and 1+1H BsAbs using an anti-mouse CD3ε (muCD3ε) antibody sequence (145-2C11) (*17*). Both formats bound muCD3ε with similar affinities (62 nM K_D for 2C11 2+2 and 95 nM for 2C11 1+1H), which were substantially lower than what was observed with the anti-huCD3ε 2+2 and 1+1H BsAbs (table S5 and fig. S1). Nevertheless, we found that the 2+2 format (0.8 pM EC_{50}) outperformed the 1+1H (9.9 pM EC_{50}), albeit to a lesser extent than we observed with the huOKT3 variants (table S4). Collectively, these results suggest that the cytotoxic advantage of 2+2 over 1+1H is at least partially due to the format of the molecule.

We next investigated whether the enhanced in vitro potency of 2+2 would translate into superior antitumor activity in vivo (Fig. 2 and figs. S2 and S3). First, we used a xenograft mouse model in immunodeficient IL-2rg$^{-/-}$ Rag2$^{-/-}$ BALB/c double knock out (DKO) mice (Fig. 2A) (*12*). DKO mice were implanted subcutaneously with human melanoma tumors (M14) and then treated intravenously with huATCs and BsAbs. 2+2 elicited strong antitumor activity, shrinking large tumors (up to 1000 mm^3) in all treated mice (Fig. 2B), whereas 1+1H failed to confer any benefit relative to a control BsAbs (an IgG-[L]-scFv directed against an irrelevant tumor antigen).

Comparing 2+2 with 1+1B in vivo was complicated by their vastly different pharmacokinetic properties; 1+1B had a short serum half-life of ~15 min (*18*) compared to ~3 days for 2+2 (table S6). To circumvent this issue, we used an ex vivo–"armed" T cell (EAT) xenograft model in which huATCs were prebound with BsAbs, washed, and then injected into neuroblastoma patient-derived xenograft (PDX)–bearing DKO mice (fig. S2A). The goal was to create chimeric antigen receptor (CAR)–like T cells that acquired their tumor-binding potential before adoptive transfer. Any differences in their subsequent antitumor function could then be directly related to the cytotoxic potency of the BsAb used to "arm" them. For these experiments, 2+2, 1+1B, and 1+1H preincubation protocols were optimized such that all EATs contained comparable amounts of anti-GD2 binding domains (fig. S2B). All three BsAbs remained stably bound to huATCs at 37°C for up to 3 days in vitro (fig. S2C), indicating that the EATs could be treated as CAR-like T cells. However, in vivo, 2+2 EAT displayed robust antitumor activity, whereas 1+1H and 1+1B EATs both failed to show any benefit (fig. S2D). These results confirm the enhanced efficacy of 2+2 and demonstrate that its superiority does not arise solely from its pharmacokinetics.

Last, we tested each of the BsAbs in a syngeneic model using C57BL/6 mice that carried a huCD3ε transgene (huCD3ε-tg) (*19*). T cells in these mice coexpressed the huCD3ε protein along with the native murine homolog, allowing our BsAbs to engage naïve T cells directly in their natural setting (fig. S3A). Despite 2+2 having bivalency toward huCD3ε, none of the mice in our syngeneic experiments

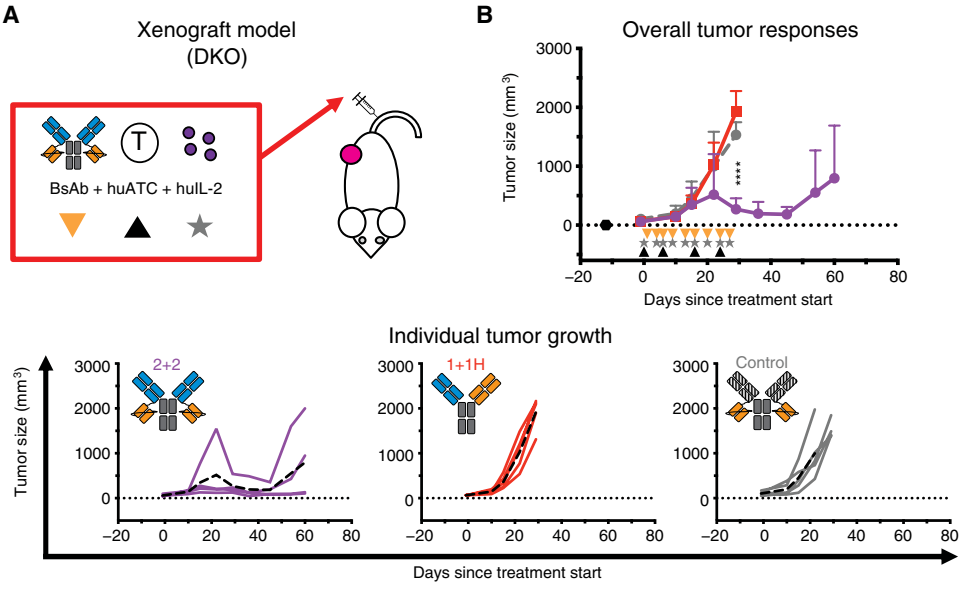

Fig. 2. In vivo comparison of IgG-[L]-scFv to common BsAb designs. (**A**) Schematic of the treatment design for the xenograft tumor model. BsAb (25 pmol) was administered intravenously twice per week (black triangle), 40 million huATCs were administered intravenously once per week (orange triangle), and human IL-2 (1000 U) was administered subcutaneously twice per week (gray star). An anti-GPA33 BsAb was used as a control. (**B**) Average (top) and individual mouse (bottom) tumor responses in each group. In the overall response graph, each line represents one treatment group ($n = 4$ to 5). The dotted black line represents no measurable tumor, and the black hexagon represents the tumor implantation. Tumor averages were calculated until at least one mouse had to be euthanized. Data are shown as means ± SD. In the individual response graphs, each line represents a single mouse, and the dashed lines represent the group average. For reference: 2+2 is purple, 1+1H is red, and the control BsAb is gray. Statistical significances were calculated by two-way analysis of variance (ANOVA) with Tukey correction. ****$P < 0.0001$ for control or 1+1H compared to 2+2.

displayed overt signs of toxicity such as weight loss or piloerection. 2+2 did induce a modest reduction in white blood cells after the first dose (fig. S3B); however, we observed a similar drop in 1+1H- and 1+1B-treated mice, implying that this was not specific to bivalent T cell engagement. Consistent with the results of the xenograft models, 2+2-treated mice displayed significant ($P < 0.0001$) growth inhibition of subcutaneous GD2$^+$ EL.4 lymphoma tumors. Neither 1+1H- nor 1+1B-treated mice showed any benefit (fig. S3C), despite daily dosing of 1+1B to mimic the continuous infusion methods used clinically, indicating that the enhanced activity of the 2+2 design applied to both naïve and preactivated T cells. Together, the results of our in vitro data and three different animal models demonstrate that the IgG-[L]-scFv format drives substantially more robust antitumor responses than either BiTE or IgG heterodimer formats.

Interdomain spacing is critical to IgG-[L]-scFv format's antitumor activity

We next evaluated two additional dual bivalent BsAb formats (Fig. 3A and table S7), an IgG-[H]-scFv (2+2HC) (*20*) and a human IgG_1-based BiTE-Fc (2+2B) (*6*). In contrast to 2+2, which used a single Ig domain (C_L) to separate tumor and T cell binding components, 2+2HC increased the spacing to three Ig domains (C_{H1}-C_{H2}-C_{H3}) by fusing each anti-huCD3ε scFv to the C terminus of each anti-GD2 heavy chain. Conversely, 2+2B used a short (G_4S_1) linker between each pair of scFv's to reduce the spacing between tumor and T cell binding domains. All three BsAb bound GD2$^+$ human M14 melanoma cells comparably in flow cytometric assays (Fig. 3B); however, their binding to T cells was unexpectedly different. 2+2B bound most effectively, displaying enhancement in both maximum binding and binding EC_{50} relative to both 2+2 and 2+2HC. 2+2HC exhibited about 10-fold greater T cell binding potency than 2+2, with comparable maximum binding. These results reveal that interdomain spacing is critical for robust T cell engagement and imply that, in contrast to the 2+2B format, 2+2 and 2+2HC may not be capable of consistent bivalent CD3 engagement.

Unexpectedly, both 2+2B and 2+2HC exhibited reduced in vitro cytotoxicity compared to 2+2 (Fig. 3C and table S7), lysing tumor cells with ~2- to ~3-fold lower potency compared to 2+2 (80 and 140 fM EC_{50}, respectively, versus 38 fM in 2+2). To further investigate these unexpected differences in in vitro function, we performed coculture assays (Fig. 3D and figs. S4 and S5) with naïve human T cells and GD2$^+$ M14 melanoma cells, using T cell activation and cytokine release as downstream readouts. 2+2 induced substantially stronger interleukin-2 (IL-2) cytokine release compared to either 2+2HC or 2+2B, in terms of both overall response and potency. 2+2 also elicited more potent up-regulation of the early response surface markers CD69 and CD25 (fig. S5A), confirming that 2+2 activated T cells more effectively than 2+2B or 2+2HC. None of the BsAbs induced measurable cytokine release or T cell activation in the absence of tumor cells (fig. S5B), demonstrating that these responses were entirely antigen dependent.

To determine the effects of interdomain spacing on in vivo tumor responses, we compared these three formats using both the conventional (Fig. 4) and the EAT (fig. S6) xenograft models. In both systems, only 2+2 elicited robust antitumor responses, whereas 2+2B and 2+2HC displayed minimal efficacy relative to untreated or unarmed controls. These results were unexpected and suggested two important points: (i) Bivalency alone was insufficient to drive strong antitumor function, and (ii) reducing interdomain spacing did not necessarily confer increased cytotoxicity. Instead, the superiority of the 2+2 design implied that optimal interdomain spacing and spatial configuration were critical for driving the most robust in vitro and in vivo antitumor responses.

Valency improves tumor and T cell binding of IgG-[L]-scFv format

To identify the properties of the IgG-[L]-scFv format responsible for its notable antitumor activity, we engineered four new IgG-[L]-scFv heterodimers (Fig. 5 and table S8), which represented all possible combinations of valency and interdomain spatial configurations. As before, heterodimers were made by first producing the necessary homodimeric parental IgG or IgG-[L]-scFv proteins containing either a K409R or an F405L substitution in the Fc region. By using a

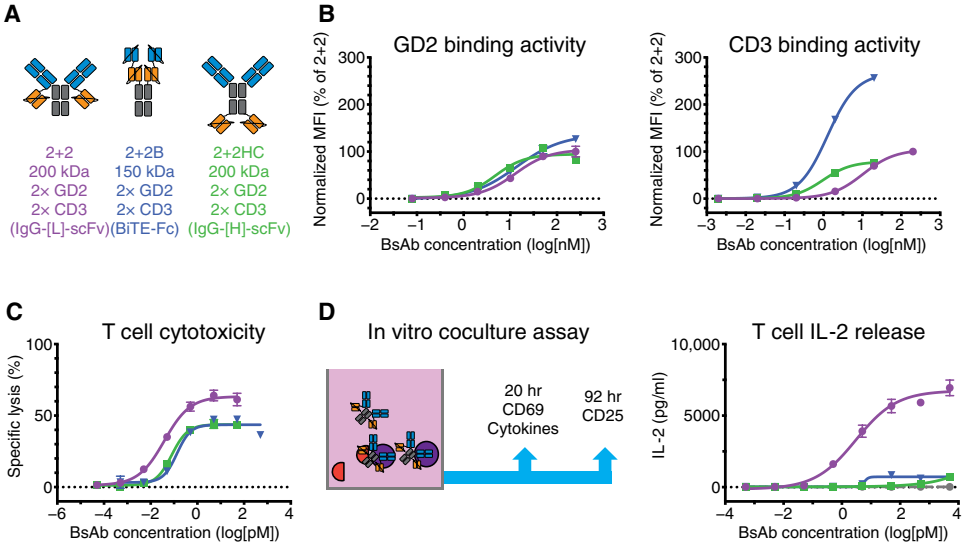

Fig. 3. Comparison of dual bivalent BsAb designs. (**A**) Schematic of dual bivalent BsAb panel: IgG-[L]-scFv (2+2), BiTE-Fc (2+2B), and IgG-[H]-scFv (2+2HC). Orange represents anti-huCD3ε domains (derived from huOKT3), and blue represents anti-GD2 domains (derived from hu3F8). (**B**) Representative cell-binding activity of each BsAb against GD2$^+$ human M14 melanoma cells (left) and CD3$^+$ huATCs (right), measured by flow cytometry. Geometric mean intensity was normalized to 2+2 (100%) for each BsAb. (**C**) Representative T cell–dependent cytotoxicity for each BsAb. (**D**) Schematic of in vitro coculture assay (left) and graph of results (right). For reference: 2+2 is purple, 2+2B is blue, and 2+2HC is green. Each curve represents one BsAb, and each point represents a single concentration, with two (FACS, cytokine) or three (cytotoxicity) technical replicates. Data are shown as means ± SD.

combination of IgG antibody and IgG-[L]-scFv BsAb directed against GD2 or an irrelevant antigen (CD33) (*10*), all possible variations of the anti-GD2 IgG-[L]-scFv format were produced (Fig. 5, A and B); 1+2 had one anti-GD2 domain replaced by a nonbinding anti-CD33 domain (humanized M195), 2+1 had one anti-huCD3ε domain removed, and each 1+1 had one anti-GD2 domain replaced and one anti-huCD3ε domain removed, either from the same side (cis) or from opposite sides (trans), hereafter named 1+1C and 1+1T, respectively. The purity of each preparation was confirmed using size exclusion chromatography–high-performance liquid chromatography and capillary zone electrophoresis to assess size and charge, respectively (table S8).

We began our comparative analyses by determining the antigen-binding affinity of all constructs by SPR (tables S9 and S10). As expected, BsAbs containing two GD2-binding Fabs (2+2 and 2+1) had higher apparent GD2 affinity (~3 nM K_D) than monovalent formats (1+2, 1+1T, 1+1C, and 1+1H; ~30 nM K_D). Similarly, BsAbs with two huCD3ε-binding scFvs (2+2 and 1+2) had higher apparent CD3 affinity (~10 nM K_D) than formats with only one (2+1, 1+1T, 1+1C, and 1+1H; 70 to 300 nM K_D). Flow cytometric evaluation of the binding activity of each BsAb against M14 melanoma cells and huATCs was consistent with the SPR data, with bivalent BsAbs exhibiting stronger binding to cell-associated antigen than their monovalent counterparts (Fig. 5C).

To assess how differences in binding to GD2 and huCD3ε might compound when both antigens were engaged simultaneously, we performed an in vitro cell-to-cell conjugate assay (Fig. 5D and fig. S7). Tumor cells and huATCs were differentially labeled with either cell trace violet or carboxyfluorescein succinimidyl ester, respectively, briefly incubated together with different concentrations of BsAb and then fixed in formaldehyde for flow cytometric analysis. 2+2 induced T cell:tumor cell conjugates most effectively in this assay, followed by 2+1. The remaining formats (1+2, 1+1T, 1+1C, and 1+1H) exhibited markedly less activity, although all performed better than a nontargeting control BsAb. These results indicated that bivalency, especially against the tumor, improved conjugate formation, an important step toward cytotoxicity. 1+1C and 1+1T were indistinguishable in their capacity to bind antigen or induce conjugates, which indicated that the spatial configuration of tumor and T cell binding domains did not affect conjugate formation.

Spatial configuration determines IgG-[L]-scFv function in vitro and in vivo

In vitro cytotoxicity assays targeting M14 melanoma cells revealed notable differences within the IgG-[L]-scFv panel (Fig. 6A and table S8). 2+2 induced the strongest antitumor cytotoxicity (26 fM EC_{50}), followed by 2+1 (240 fM EC_{50}) and 1+2 (773 fM EC_{50}), which were ~9-fold and ~30-fold less effective, respectively. Unexpectedly, 1+1C (780 fM EC_{50}) was essentially equipotent to 1+2, despite having markedly less binding activity to huCD3ε. The potency of 1+1T (37 pM EC_{50}), by contrast, was similar to that of 1+1H (20 pM EC_{50}), which was ~50-fold worse than 1+2 and 1+1C, and more than 1000-fold worse than 2+2. To confirm that these results were not GD2 specific, we performed reciprocal cytotoxicity experiments targeting CD33. Because an anti-CD33 Fab was used as the control arm for the anti-GD2 IgG-[L]-scFv panel, only two additional heterodimers needed to be made for these studies—CD33 2+1 and CD33 1+1H—whereas 1+2, 1+1T, and 1+1C from the GD2 panel could be directly applied. CD33 2+2 (0.9 pM EC_{50}) was the most potent design, followed by CD33 2+1 (4.5 pM EC_{50}), 1+2 (6.0 pM EC_{50}), CD33 1+1C (aka GD2 1+1T, 11.5 pM EC_{50}), CD33 1+1H (134 pM EC_{50}), and lastly CD33 1+1T (aka GD2 1+1C, 500 pM EC_{50}) (table S11). This confirmed that the rank order of cytotoxic activity exhibited by the various IgG-[L]-scFv variants was a generalizable property of format architecture and not specific to the tumor antigen.

To explore how differences in valency and spatial configuration affected naïve T cell activation, we compared the panel of IgG-[L]-scFv using an in vitro coculture assay (Fig. 6, B to F, and figs. S4 and S8). Once more, IL-2 secretion revealed major differences between the different BsAb variants. 2+2 elicited substantially stronger IL-2 secretion than all other BsAbs, displaying nearly 100-fold higher potency than the next most stimulatory variant (Fig. 6B). 2+1, 1+2, and 1+1C exhibited intermediate potencies, and 1+1T and 1+1H induced weak IL-2 secretion near the lower limit of detection. T cell activation and proliferation generally followed the same rank order, although with smaller differences, and remained consistent for both CD4$^+$ and CD8$^+$ T cell subsets (Fig. 6, C to F, and fig. S8, A and B). 2+2 displayed the highest potency, whereas 1+1T was consistently the weakest variant, indistinguishable from 1+1H and about 200-fold less

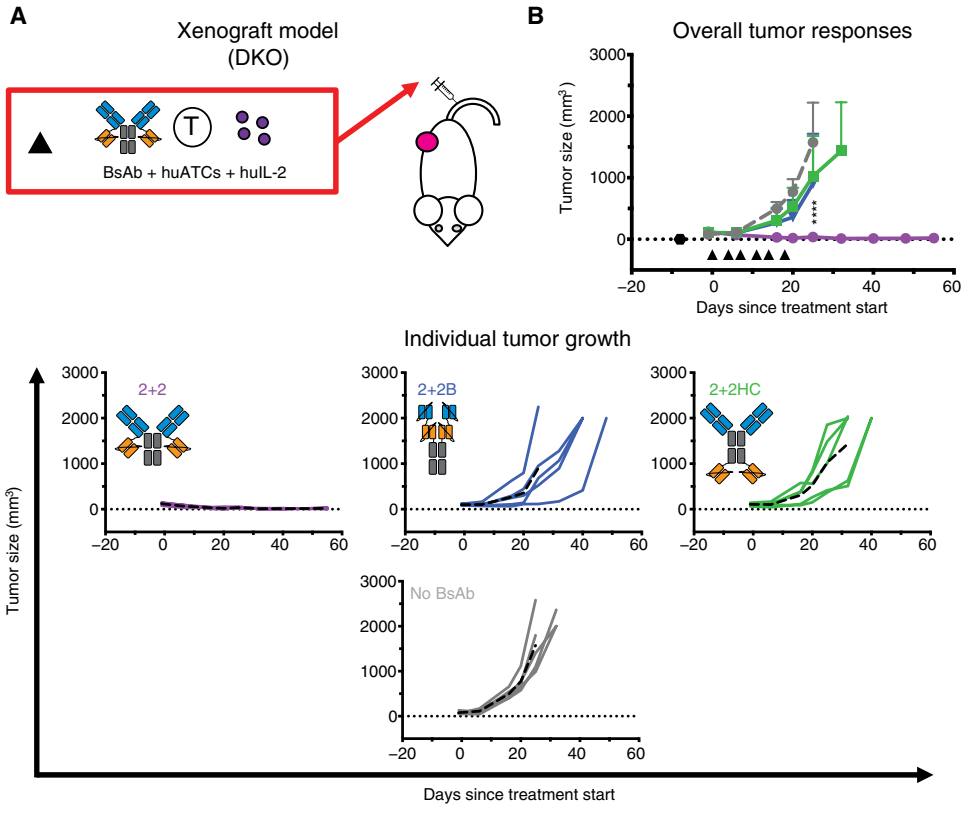

Fig. 4. In vivo tumor responses of dual bivalent BsAb designs. (**A**) Schematic of the treatment design for the xenograft tumor model. BsAb (10 pmol) was administered intravenously twice per week along with 20 million huATCs and subcutaneous human IL-2 (1000 U) (black triangle). (**B**) Average (top) and individual mouse (bottom) tumor responses in each group. In the overall response graph, each line represents one treatment group ($n = 5$). The dotted black line represents no measurable tumor, and the black hexagon represents the tumor implantation. Tumor averages were calculated until at least one mouse had to be euthanized. Data are shown as means ± SD. In the individual response graphs, each line represents a single mouse, and the dashed lines represent the group average. For reference: 2+2 is purple, 2+2B is blue, 2+2HC is green, and the control group (no BsAb) is gray. Statistical significances were calculated by two-way ANOVA with Tukey correction. ****$P < 0.0001$ for control, 2+2HC, or 2+2B compared to 2+2.

stimulatory than 2+2. 2+1, 1+2, and 1+1C generally clustered together at intermediate potencies, with 2+1 displaying slightly more effective activation, followed by 1+2 and then 1+1C. As before, T cells incubated with BsAb, but without tumor cells, did not exhibit any measurable responses (fig. S8C), indicating that BsAb-mediated T cell activation was antigen dependent.

The consistent and notable differences in efficacy between 1+1C and 1+1T suggested that the spatial configuration of antigen-binding domains was a key determinant of BsAb activity in vitro. Furthermore, whereas 2+2 displayed clear benefits over 2+1 and 1+2, neither 2+1 nor 1+2 was superior to 1+1C. Hence, the addition of antigen-binding domains improved function most effectively when it created an additional cis-module. Together, these data demonstrate that dual bivalency within the IgG-[L]-scFv framework enhances BsAb function by improving cell binding and presenting tumor and T cell binding domains in cis-configuration.

To determine the effects of valency and spatial configuration on in vivo tumor responses, we examined the IgG-[L]-scFv panel using both xenograft and syngeneic tumor models (Fig. 7 and fig. S9). In DKO mice bearing subcutaneous human melanoma (M14) tumors and treated with BsAb and huATCs (Fig. 7A), 2+2 again displayed the strongest antitumor activity (Fig. 7B). 2+1 initially elicited similar responses to 2+2 but ultimately had inferior durability, with tumors recurring quickly after treatment ended. Consistent with the in vitro functional studies, 1+2 and 1+1C both exhibited moderate antitumor activity, but they were noticeably worse than 2+1 and 2+2. Last, both 1+1H and 1+1T failed to show any antitumor efficacy relative to mice treated with control BsAb.

Results were more polarized in the syngeneic model (fig. S9A). Here, only 2+2 displayed measurable antitumor activity, whereas all other BsAbs completely failed to inhibit tumor growth (fig. S9B). None of the BsAb-treated mice displayed any indices of toxicity, such as weight loss or piloerection. Although all members of the IgG-[L]-scFv panel modestly increased plasma IL-6, they did so to a much lesser extent than did a positive control reagent containing a full-length OKT3 IgG antibody (fig. S9C) (*21*), indicating that the IgG-[L]-scFv design did not elicit measurable amounts of antigen-independent activation or cytokine release and further demonstrating that bivalency against CD3 in the IgG-[L]-scFv design was safe and effective. Collectively, these results are consistent with our in vitro findings and confirm the importance of cis-configured tumor and T cell binding domains.

DISCUSSION

In this study, we directly examined how the IgG-[L]-scFv design improved antitumor responses compared to multiple other formats targeted against both GD2 and CD33. We found that dual bivalency was crucial for function but unexpectedly not for the reasons we had initially anticipated. Although bivalency had the expected effect of enhancing binding against both tumor cells and T cells, several of our results indicated that this was of secondary importance therapeutically. For instance, although 2+2B (BiTE-Fc) and 2+2HC (IgG-[H]-scFv) exhibited similar tumor binding and superior T cell binding relative to 2+2, both failed to show antitumor activity in vivo. Furthermore, adding a second antitumor Fab (GD2 or CD33) to 1+1C (to generate 2+1) provided only a modest improvement in activity, and adding a second anti-huCD3ε scFv to 1+1C (to generate 1+2) made essentially no difference. Effective in vitro and in vivo antitumor activities were better correlated with two other properties: (i) the spatial orientation of tumor and T cell binding domains in a cis-configuration and (ii) their separation by a single Ig spacer (C_L). Using these two criteria, all tested formats are easily grouped into a rank order of ascending efficacy: zero cis-modules (low potency): 1+1T and 1+1H; two cis-modules with suboptimal interdomain

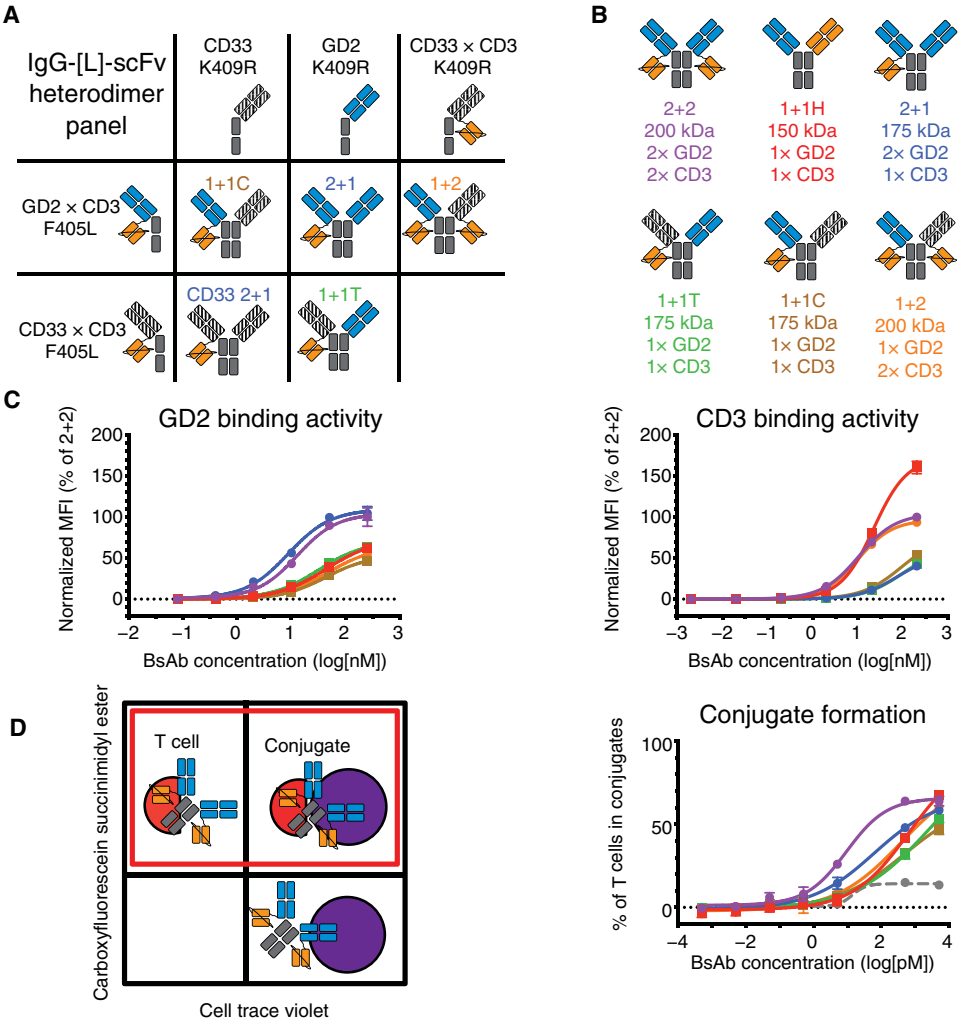

Fig. 5. In vitro binding activity of IgG-[L]-scFv panel. (**A**) Schematic of heterodimerization strategy for the IgG-[L]-scFv panel. (**B**) Resulting IgG-[L]-scFv panel: 2+2, 1+1H, 2+1, 1+1T, 1+1C, and 1+2. Orange domains represent anti-huCD3ε domains (derived from huOKT3), blue domains represent anti-GD2 domains (derived from hu3F8), and black striped domains represent irrelevant anti-CD33 domain (derived from huM195). (**C**) Representative cell-binding activity of each BsAb against $GD2^+$ human M14 melanoma cells (left) and $CD3^+$ huATCs (right), measured by flow cytometry. Geometric mean intensity was normalized to 2+2 (100%) for each BsAb. (**D**) Schematic of conjugate assay analysis (left) and graph of results (right). Unconjugated cells (upper left and lower right quadrants) displayed fluorescence under one channel, whereas conjugated cells (upper right quadrant) displayed fluorescence under two channels. For analysis, conjugate frequency was measured as the fraction of conjugated T cells among the total T cells (red box). An anti-CD33 BsAb was used as a control. Graphed values represent the amount of conjugate formation at each concentration of BsAb. For reference: 2+2 is purple, 1+1H is red, 2+1 is blue, 1+1T is green, 1+1C is brown, 1+2 is orange, and the control BsAb is gray. Each curve represents one BsAb, and each point represents a single concentration, with two technical replicates. Data are shown as means ± SD.

spacing (low-moderate potency): 2+2B and 2+2HC; one cis-module with optimal interdomain spacing (moderate potency): 2+1, 1+2, and 1+1C; and two cis-modules with optimal interdomain spacing (high potency): 2+2. Moreover, the beneficial effects of cis-configurations and interdomain spacing that we have observed are consistent with a recent report describing a high-potency T cell BsAb containing a single cis-module (Fab-Fab) (*22*). We conclude that, in the case of T cell BsAb, the total number of interactions matters less than the way those interactions are made.

Although most of our experiments used reagents derived from 3F8 (anti-GD2) and OKT3 (anti-huCD3), other sequences were also examined to assess the generalizability of our findings. Although we were able to corroborate key observations using BsAb based on clone M195 (targeting CD33 on tumors), the functional advantage of the 2+2 format was less pronounced when we used an alternative CD3-binding clone (145-2C11, targeting murine CD3) to engage T cells. Here, note that many other anti-CD3 sequences are under development in T cell BsAbs, and it is possible that some may behave differently from OKT3 within the IgG-[L]-scFv design, depending on their binding affinity and epitope. A more thorough examination of the 2+2 design with additional anti-CD3 modules would be an interesting topic for future research. Nevertheless, we feel that our findings are broadly relevant to clinical practice, in particular, because OKT3 continues to be one of the most clinically used sequences in T cell BsAbs (*7*) and is the backbone of the only FDA-approved T cell BsAb, blinatumomab (which uses L2K, a minor variant) (*23*).

The comparison of BsAbs in both syngeneic and xenograft animal models also revealed important differences between the various formats. It is tempting to speculate that among the tested designs, only the IgG-[L]-scFv had the stimulatory power to elicit productive in vivo responses from naïve T cells, which are more difficult to activate than effector T cells and take a longer time to respond. It is also notable that the capacity of each BsAb to elicit antigen-dependent IL-2 release from T cells in vitro was the best predictor of in vivo activity in all animal models. This strong correlation between in vivo potency and in vitro IL-2 production from naïve T cells highlights the importance of T cell cytokines as components of productive antitumor responses in addition to being biomarkers of T cell activation. Although recent work (*24*) has suggested that antileukemia activity may not require strong cytokine release, our data suggested that robust responses against solid tumors required potent IL-2 secretion. In light of these results, it may be worth reevaluating design strategies aimed at minimizing cytokine production to mitigate side effects (*25*), because these same strategies might compromise clinical antitumor efficacy.

Prior studies have demonstrated that BsAb-targeting epitopes close to the tumor cell membrane (proximal) elicited more potent T cell cytotoxicity than those that bound epitopes farther away (distal) (*26*, *27*), implying that close apposition between T cells and tumor cells drives more effective T cell activation and killing. This phenomenon

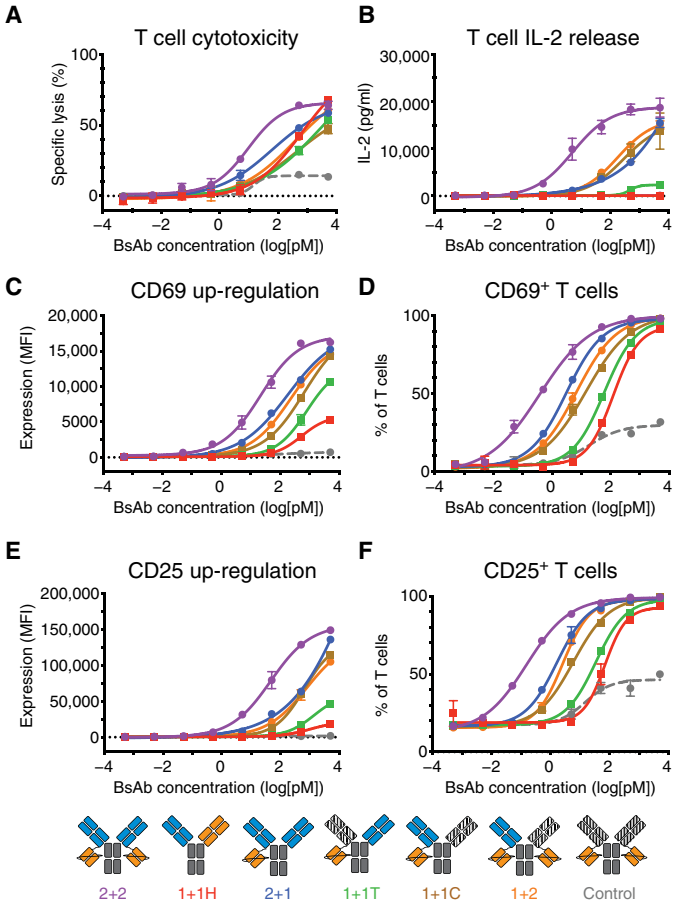

Fig. 6. In vitro functional activity of IgG-[L]-scFv panel. (**A**) Representative T cell–dependent cytotoxicity of each BsAb. (**B** to **E**) T cell activation data from coculture assays. (B) IL-2 cytokine release after 20 hours of coculture. (C) CD69 expression intensity and (D) frequency of expression on T cells after 20 hours of coculture. (E) CD25 expression intensity and (F) frequency of expression on T cells after 92 hours of coculture. Assays included an anti-CD33 BsAb as a control. Schematic (bottom) for reference: 2+2 is purple, 1+1H is red, 2+1 is blue, 1+1T is green, 1+1C is brown, 1+2 is orange, and the control BsAb is gray. Each curve represents one BsAb, and each point represents a single concentration, with two (cytokine) or three (cytotoxicity) technical replicates. Data are shown as means ± SD.

has been linked to the exclusion of the inhibitory phosphatase CD45 (*27*), which contains a large extracellular domain that cannot fit into tight intercellular spaces. Although this could explain why the cis-configured 1+1C performs better than the trans-configured 1+1T in our hands, the superiority of the 2+2 (IgG-[L]-scFv) format over the 2+2B (BiTE-Fc) design indicates that minimizing the distance between tumor antigen and T cell binding domains does not always improve BsAb performance. In that regard, note that the T cell receptor (TCR) is a mechanosensitive protein that undergoes activating conformational changes in response to forces applied to its ligand-binding domain (*28*, *29*). Hence, the interdomain spacing imparted by a C_L domain in the IgG-[L]-scFv format may provide the most optimal physical constraint or mechanical coupling between the TCR and tumor cell, resulting in stronger and/or more sustained delivery of activating signals. Comparing the capacity of different BsAb formats to induce TCR conformational change will be an interesting topic for future work.

Our study also strongly supports the feasibility of developing BsAbs with bivalency toward T cells. Although many BsAb designs currently in clinical development use tumor bivalency to increase potency (*22*, *30*) or to improve selectivity (*31*), bivalency against T cell epitopes has largely been avoided for fear of nonspecific activation (*32*). We found, however, that the additional cis-module generated by adding a second anti-CD3 scFv to 2+1 markedly improved both in vitro and in vivo functionality (compare 2+1 to 2+2) without inducing toxicity. Although 2+2 did show superior T cell binding compared to 2+1, it was inferior to both 2+2B and 2+2HC, which also contained two anti-CD3 scFv domains. We can only speculate as to why 2+2 binds T cells less strongly than the other bivalent BsAbs. It may be that the IgG-[L]-scFv format imparts structural constraints, not present in the 2+2B or the 2+2HC designs, that impede consistent bivalent T cell engagement. What is clear from our results, however, is that 2+2 outperformed both 2+2B and 2+2HC in antitumor function. Hence, T cell bivalency, when combined with the proper interdomain spacing and spatial configuration, can afford critical improvements in activity that are independent of its capacity to enhance T cell binding. Last, as a dual bivalent design, the IgG-[L]-scFv format gains the added benefit of being symmetrical and is therefore less complicated to manufacture relative to asymmetrical designs that combine tumor bivalency with T cell monovalency.

Note also that monovalent T cell engagement does not necessarily eliminate clinical toxicities such as cytokine release or antigen-independent immune activation. Many dual monovalent formats such as blinatumomab, the FDA-approved anti-CD19 BiTE, or tandem-scFv BsAbs targeting CD123 induced substantial cytokine release or neurotoxicity during their clinical development (*33*–*37*), although this has been ameliorated by the use of tocilizumab and pretreatment with steroids (*38*). Although the added complexity of extra binding domains might be expected to complicate clinical grade development (by compromising stability or reagent purity) or increase immunogenicity, relative to monovalent designs, we have not observed these issues when generating clinical-scale quantities of the anti-GD2 IgG-[L]-scFv BsAb. A phase I clinical trial of the GD2-specific 2+2 is currently underway (NCT03870207), and it will be interesting to compare any immune-mediated side effects with those that have been reported for monovalent BsAb.

Despite 30 years of development, to date, only one T cell BsAb has been clinically approved by the FDA, with most failing due to insufficient potency in the face of dose-limiting toxicities (typically cytokine release related). Here, we have shown that cis-configured binding domains and dual bivalency can provide log-fold improvements to T cell BsAb potencies in vitro and superior efficacies in vivo. If incorporated into future BsAb design strategies, these conceptual guidelines may substantially improve clinical outcomes. Although the IgG-[L]-scFv design may not be optimal for all anti-CD3 sequences, or against certain classes of tumor antigens (large bulky proteins, secreted or cleaved epitopes, etc.), we believe that it represents a good standard for most T cell–engaging BsAbs and is a marked improvement over many other conventional formats. By combining the benefits of symmetry (2+2), spatial configuration (cis), interdomain spacing (C_L), and pharmacokinetics (IgG-like), an OKT3-based IgG-[L]-scFv could potentially drive forward both clinical progress and academic studies in coming years.

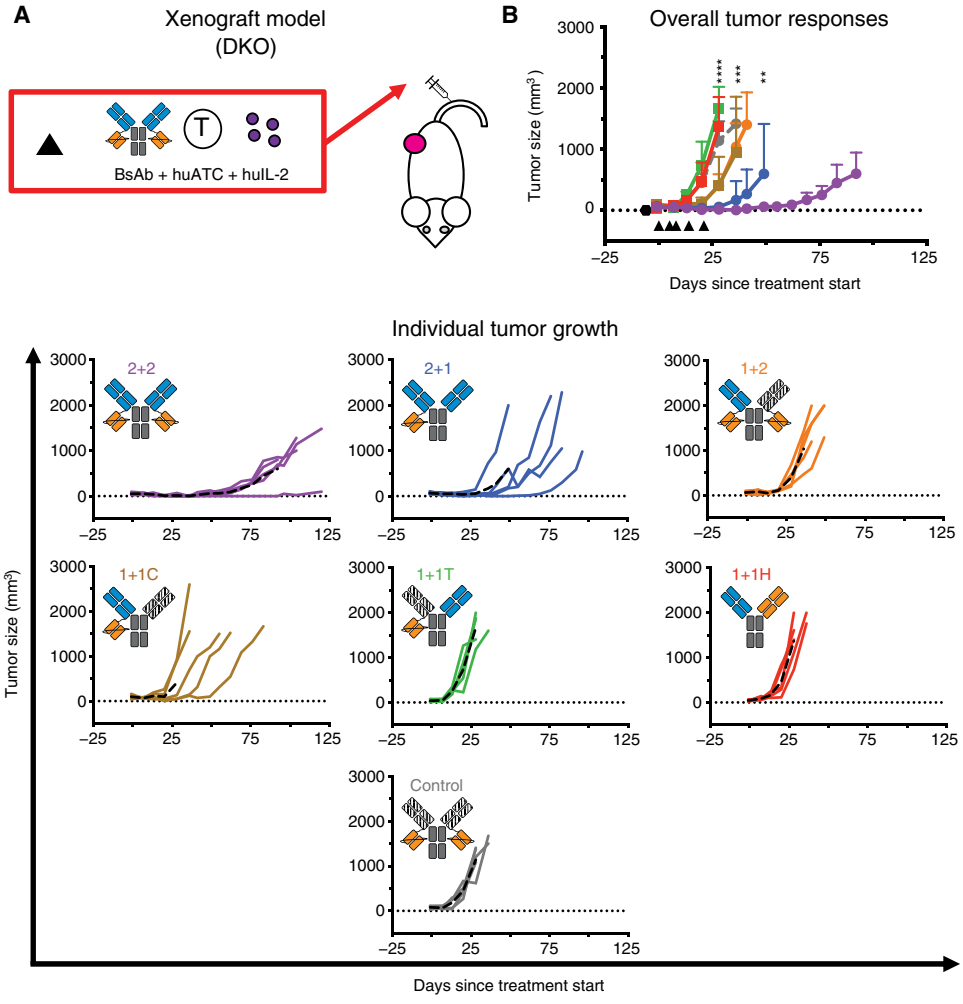

Fig. 7. In vivo antitumor activity of IgG-[L]-scFv panel. (**A**) Schematic of the treatment design for the xenograft tumor model. BsAb (25 pmol) was administered intravenously twice per week along with 20 million huATCs and subcutaneous and human IL-2 (1000 U) (black triangle). An anti-CD33 BsAb was used as a control. (**B**) Average (top) and individual mouse (bottom) tumor responses in each group. In the overall response graph, each line represents one treatment group ($n = 5$). The dotted black line represents no measurable tumor, and the black hexagon represents the tumor implantation. Tumor averages were calculated until at least one mouse had to be euthanized. Data are shown as means ± SD. In the individual response graphs, each line represents a single mouse, and the dashed lines represent the group average. For reference: 2+2 is purple, 1+1H is red, 2+1 is blue, 1+1T is green, 1+1C is brown, 1+2 is orange, and control BsAb is gray. Statistical significances were obtained by two-way ANOVA and Tukey correction. ****$P < 0.0001$ for control, 1+1H, and 1+1T compared to 1+2, 1+1C, 2+1, or 2+2. ***$P < 0.001$ for 1+2 or 1+1C compared to 2+1 or 2+2. **$P < 0.01$ for 2+1 compared to 2+2.

MATERIALS AND METHODS

Study design

The primary objective of this study was to identify the effects of BsAb format on in vitro and in vivo antitumor function. We compared nine BsAb formats using human and murine T cells, cell lines, and human PDX tumors.

For in vivo experiments, sample sizes were determined on the basis of the observed variation in tumor progression and response in previous studies (*9*, *12*, *13*). Four to five animals were used for each group in every animal experiment. Mice were followed until tumors became too large (>1500 mm^3), and no data were excluded. All mice from the same treatment groups were cohoused in the same cage. Experiments using female mice were completely randomized after tumor implantation but before their initial treatment. Experiments using male mice had cages randomized after tumor implantation and before the start of treatment. Blinding of treatment or experimental measurements was not performed.

Animal studies

All experiments were performed in compliance with all relevant ethical regulations and in accordance with an Institutional Animal Care and Use Committee–approved protocol (protocol 09-05-010). All mice used in treatment studies were bred in the Memorial Sloan Kettering Cancer Center (MSKCC) animal facility. Mice for pharmacokinetic analysis were purchased. Weights and tumor volumes were measured once per week, and overall mouse health was evaluated at least three times per week. Tumor volumes were calculated using a TM900 measurement device (Peira) or caliper. For caliper measurements, volume measurements were estimated as $[(L) \times (W) \times (W) \times 0.5]$, where L is the longest diameter of the tumor, and W is the diameter perpendicular to L. Mice were euthanized once tumor volumes reached 1.5 to 2.0 cm^3. No treatment-related toxicities (weight loss, hair loss, weakness, etc.) were observed in any mice throughout these experiments.

The three mouse models used were as follows: (i) an immunodeficient xenograft model (*12*), (ii) an immunodeficient armed T cell xenograft model (*21*), and (iii) an immunocompetent huCD3ε-transgenic syngeneic model (*19*). In the first model, 8- to 16-week-old male DKO (Taconic, 11503) mice were implanted subcutaneously with M14 melanoma cells or IMR32 neuroblastoma cells. After 5 to 15 days (tumors about 100 to 200 mm^3), mice were treated intravenously with huATCs (40 or 20 million cells, once or twice per week, respectively), intravenously with BsAb (10 to 25 pmol, twice per week), and subcutaneously with human IL-2 (aldesleukin, 1000 U, twice per week) for 3 weeks.

For the second model, 10- to 16-week-old male or female DKO mice were implanted with digested PDX tumors (each tumor was passaged into 10 new mice). Treatment began 8 to 20 days after implantation. For each treatment, huATCs were incubated in vitro with each BsAb for 20 min at room temperature. After the incubation, cells were washed once and injected intravenously into xenografted mice (20 million cells, twice per week) along with subcutaneous IL-2 (aldesleukin, 1000 U, twice per week) for 3 weeks.

For the third model, B6.Cg-Tg(CD3E)600Cpt/J (huCD3ε-tg; The Jackson Laboratory, 020456) mice were bred with wild-type

C57BL/6 mice (The Jackson Laboratory, 000664) to generate huCD3ε-tg F1 heterozygotes, which were used for all experiments. From here, 8- to 16-week-old male mice were implanted subcutaneously with 50000 EL.4 lymphoma cells. After 7 days, mice were treated intravenously with BsAb (25 pmol, twice per week) for 3 weeks. The BiTE was dosed daily (7 pmol per dose) for 3 weeks to account for poorer pharmacokinetics.

All cell line implantations used Matrigel (Corning, 354234) at a ratio of 3:1 by volume (Matrigel to cells). PDX tumors were implanted by the antitumor assessment core facility at MSKCC. Plasma was collected retro-orbitally and stored at −80°C until assayed. Complete blood count measurements were performed on freshly collected whole blood (EDTA neutralized) using an HT5 Hematology Analyzer (Heska) in the antitumor assessment core facility. Data were plotted using GraphPad Prism 8.

Pharmacokinetic analysis

Female Balb/c nude mice [Envigo, 069(nu)/070(nu/+)] were injected with 100 μg of BsAb or monoclonal antibody (mAb) and bled serially over 7 days (30 min to 168 hours). Blood was processed as serum and frozen until all samples were acquired. Serum concentrations of BsAb or mAb were determined by enzyme-linked immunosorbent assay. Briefly, wells were coated with anti-3F8 idiotype antibody (50 μl, 20 μg/ml) overnight at room temperature. After this, plates were washed with phosphate-buffered saline (PBS) and blocked with PBS supplemented with 0.5% bovine serum albumin (Sigma, A7906) for 1 hour at room temperature. Serum samples were added at dilutions of 1:100 and 1:1000 in duplicate and incubated at 37°C for 2.5 hours. Samples were then detected with a mouse anti-human Fc-specific secondary antibody conjugated with horseradish peroxidase (SouthernBiotech, clone 4E3, 9052-05) for 1 hour at 4°C. Plates were developed with *o*-phenylenediamine (Sigma, P8287-100TAB) and stopped with 5 N sulfuric acid. Plates were read at 490 nm using a BioTek H1 plate reader (Synergy) with the Gen5 software (version v2.09). Protein concentrations were calculated using a standard curve of either 2+2 or hu3F8 IgG, fitted using a three-parameter logistic fitting. Pharmacokinetic analysis was carried out by noncompartmental analysis of the serum concentration–time data using WinNonlin software program (Pharsight Corp.).

Statistical analyses

All statistical analyses were performed using Prism software version 8.0 (GraphPad). *P* values for comparisons between multiple groups were determined by two-way analysis of variance (ANOVA) with subsequent Tukey correction. For all statistical tests, a *P* value of < 0.05 was used to denote statistical significance. All error bars denote the SD, unless otherwise noted in the figure legends. Original data are in data file S1.

SUPPLEMENTARY MATERIALS

stm.sciencemag.org/cgi/content/full/12/534/eaax1315/DC1
Materials and Methods
Fig. S1. In vitro binding activity of murine T cell BsAb panel.
Fig. S2. In vivo tumor responses using EAT xenograft tumor model.
Fig. S3. In vivo tumor responses using syngeneic tumor model.
Fig. S4. In vitro coculture assay analysis.
Fig. S5. Naïve T cell activation by dual bivalent BsAb formats.
Fig. S6. In vivo tumor responses using EAT xenograft tumor model.
Fig. S7. In vitro conjugate assay analysis.
Fig. S8. T cell activation using the IgG-[L]-scFv panel.
Fig. S9. In vivo tumor responses using syngeneic tumor model.
Table S1. In vitro properties and design of anti-GD2 BsAb.
Table S2. GD2 binding kinetics for BsAb using SPR.
Table S3. huCD3ε binding kinetics for BsAb using SPR.
Table S4. In vitro properties and design of additional anti-GD2 BsAb.
Table S5. muCD3ε binding kinetics for BsAb using SPR.
Table S6. In vivo pharmacokinetics of 2+2 BsAb.
Table S7. In vitro properties and design of dual bivalent BsAb.
Table S8. In vitro properties and design of anti-GD2 IgG-[L]-scFv panel.
Table S9. GD2 binding kinetics for IgG-[L]-scFv panel using SPR.
Table S10. huCD3ε binding kinetics for IgG-[L]-scFv panel using SPR.
Table S11. In vitro properties and design of anti-CD33 IgG-[L]-scFv panel.
Data file S1. Original data.

View/request a protocol for this paper from *Bio-protocol*.

REFERENCES AND NOTES

1. M. Shima, H. Hanabusa, M. Taki, T. Matsushita, T. Sato, K. Fukutake, N. Fukazawa, K. Yoneyama, H. Yoshida, K. Nogami, Factor VIII–mimetic function of humanized bispecific antibody in hemophilia A. *N. Engl. J. Med.* **374**, 2044–2053 (2016).
2. M. S. Topp, N. Gökbuget, A. S. Stein, G. Zugmaier, S. O'Brien, R. C. Bargou, H. Dombret, A. K. Fielding, L. Heffner, R. A. Larson, S. Neumann, R. Foà, M. Litzow, J.-M. Ribera, A. Rambaldi, G. Schiller, M. Brüggemann, H. A. Horst, C. Holland, C. Jia, T. Maniar, B. Huber, D. Nagorsen, S. J. Forman, H. M. Kantarjian, Safety and activity of blinatumomab for adult patients with relapsed or refractory B-precursor acute lymphoblastic leukaemia: A multicentre, single-arm, phase 2 study. *Lancet Oncol.* **16**, 57–66 (2015).
3. T. Ishiguro, Y. Sano, S.-i. Komatsu, M. Kamata-Sakurai, A. Kaneko, Y. Kinoshita, H. Shiraiwa, Y. Azuma, T. Tsunenari, Y. Kayukawa, Y. Sonobe, N. Ono, K. Sakata, T. Fujii, Y. Miyazaki, M. Noguchi, M. Endo, A. Harada, W. Frings, E. Fujii, E. Nanba, A. Narita, A. Sakamoto, T. Wakabayashi, H. Konishi, H. Segawa, T. Igawa, T. Tsushima, H. Mutoh, Y. Nishito, M. Takahashi, L. Stewart, E. ElGabry, Y. Kawabe, M. Ishigai, S. Chiba, M. Aoki, K. Hattori, J. Nezu, An anti–glypican 3/CD3 bispecific T cell–redirecting antibody for treatment of solid tumors. *Sci. Transl. Med.* **9**, eaal4291 (2017).
4. S. M. Cheal, H. Xu, H.-f. Guo, P. B. Zanzonico, S. M. Larson, N.-K. Cheung, Preclinical evaluation of multistep targeting of diasialoganglioside GD2 using an IgG-scFv bispecific antibody with high affinity for GD2 and DOTA metal complex. *Mol. Cancer Ther.* **13**, 1803–1812 (2014).
5. U. Brinkmann, R. E. Kontermann, The making of bispecific antibodies. *MAbs* **9**, 182–212 (2017).
6. C. Spiess, Q. Zhai, P. J. Carter, Alternative molecular formats and therapeutic applications for bispecific antibodies. *Mol. Immunol.* **67**, 95–106 (2015).
7. Z. Wu, N. V. Cheung, T cell engaging bispecific antibody (T-BsAb): From technology to therapeutics. *Pharmacol. Ther.* **182**, 161–175 (2018).
8. A. M. Cuesta, N. Sainz-Pastor, J. Bonet, B. Oliva, L. Alvarez-Vallina, Multivalent antibodies: When design surpasses evolution. *Trends Biotechnol.* **28**, 355–362 (2010).
9. M. Cheng, B. H. Santich, H. Xu, M. Ahmed, M. Huse, N.-K. Cheung, Successful engineering of a highly potent single-chain variable-fragment (scFv) bispecific antibody to target disialoganglioside (GD2) positive tumors. *Oncoimmunology* **5**, e1168557 (2016).
10. S. S. Hoseini, H. Guo, Z. Wu, M. N. Hatano, N. V. Cheung, A potent tetravalent T-cell–engaging bispecific antibody against CD33 in acute myeloid leukemia. *Blood Adv.* **2**, 1250–1258 (2018).
11. Z. Wu, H.-F. Guo, H. Xu, N.-K. V. Cheung, Development of a tetravalent anti-GPA33/anti-CD3 bispecific antibody for colorectal cancers. *Mol. Cancer Ther.* **17**, 2164–2175 (2018).
12. A. Lopez-Albaitero, H. Xu, H. Guo, L. Wang, Z. Wu, H. Tran, S. Chandarlapaty, M. Scaltriti, Y. Janjigian, E. de Stanchina, N. -K. V. Cheung, Overcoming resistance to HER2-targeted therapy with a novel HER2/CD3 bispecific antibody. *Oncoimmunology* **6**, e1267891 (2017).
13. H. Xu, M. Cheng, H. Guo, Y. Chen, M. Huse, N.-K. V. Cheung, Retargeting T cells to GD2 pentasaccharide on human tumors using Bispecific humanized antibody. *Cancer Immunol. Res.* **3**, 266–277 (2015).
14. N.-K. Cheung, H. Guo, J. Hu, D. V. Tassev, I. Y. Cheung, Humanizing murine IgG3 anti-GD2 antibody m3F8 substantially improves antibody-dependent cell-mediated cytotoxicity while retaining targeting in vivo. *Oncoimmunology* **1**, 477–486 (2012).
15. J. R. Adair, D. S. Athwal, M. W. Bodmer, S. M. Bright, A. M. Collins, V. L. Pulito, P. E. Rao, R. Reedman, A. L. Rothermel, D. Xu, Humanization of the murine anti-human CD3 monoclonal antibody OKT3. *Hum. Antibodies Hybridomas* **5**, 41–47 (1994).
16. A. F. Labrijn, J. I. Meesters, P. Priem, R. N. de Jong, E. T. van den Bremer, M. D. van Kampen, A. F. Gerritsen, J. Schuurman, P. W. H. I. Parren, Controlled Fab-arm exchange for the generation of stable bispecific IgG1. *Nat. Protoc.* **9**, 2450–2463 (2014).
17. O. Leo, M. Foo, D. H. Sachs, L. E. Samelson, J. A. Bluestone, Identification of a monoclonal antibody specific for a murine T3 polypeptide. *Proc. Natl. Acad. Sci. U.S.A.* **84**, 1374–1378 (1987).

18. M. Ahmed, M. Cheng, I. Y. Cheung, N. K. Cheung, Human derived dimerization tag enhances tumor killing potency of a T-cell engaging bispecific antibody. *Oncoimmunology* **4**, e989776 (2015).
19. P. C. Gedeon, T. H. Schaller, S. K. Chitneni, B. D. Choi, C. -T. Kuan, C. M. Suryadevara, D. J. Snyder, R. J. Schmittling, S. E. Szafranski, X. Cui, P. N. Healy, J. E. Herndon II, R. E. McLendon, S. T. Keir, G. E. Archer, E. A. Reap, L. Sanchez-Perez, D. D. Bigner, J. H. Sampson, A rationally designed fully human EGFRvIII:CD3-targeted bispecific antibody redirects human T cells to treat patient-derived intracerebral malignant glioma. *Clin. Cancer Res.* **24**, 3611–3631 (2018).
20. M. J. Coloma, S. L. Morrison, Design and production of novel tetravalent bispecific antibodies. *Nat. Biotechnol.* **15**, 159–163 (1997).
21. M. Yankelevich, S. V. Kondadasula, A. Thakur, S. Buck, N. -K. V. Cheung, L. G. Lum, Anti-CD3 × anti-GD2 bispecific antibody redirects T-cell cytolytic activity to neuroblastoma targets. *Pediatr. Blood Cancer* **59**, 1198–1205 (2012).
22. M. Bacac, S. Colombetti, S. Herter, J. Sam, M. Perro, S. Chen, R. Bianchi, M. Richard, A. Schoenle, V. Nicolini, S. Diggelmann, F. Limani, R. Schlenker, T. Hüsser, W. Richter, K. Bray-French, H. Hinton, A. M. Giusti, A. Freimoser-Grundschober, L. Lariviere, C. Neumann, C. Klein, P. Umaña, CD20-TCB with obinutuzumab pretreatment as next-generation treatment of hematologic malignancies. *Clin. Cancer Res.* **24**, 4785–4797 (2018).
23. T. Dreier, G. Lorenczewski, C. Brandl, P. Hoffmann, U. Syring, F. Hanakam, P. Kufer, G. Riethmuller, R. Bargou, P. A. Baeuerle, Extremely potent, rapid and costimulation-independent cytotoxic T-cell response against lymphoma cells catalyzed by a single-chain bispecific antibody. *Int. J. Cancer* **100**, 690–697 (2002).
24. N. D. Trinklein, D. Pham, U. Schellenberger, B. Buelow, A. Boudreau, P. Choudhry, S. C. Clarke, K. Dang, K. E. Harris, S. Iyer, B. Jorgensen, P. P. Pratap, U. S. Rangaswamy, H. S. Ugamraj, O. Vafa, A. P. Wiita, W. van Schooten, R. Buelow, S. Force Aldred, Efficient tumor killing and minimal cytokine release with novel T-cell agonist bispecific antibodies. *MAbs* **11**, 639–652 (2019).
25. D. Ellerman, Bispecific T-cell engagers: Towards understanding variables influencing the in vitro potency and tumor selectivity and their modulation to enhance their efficacy and safety. *Methods* **154**, 102–117 (2019).
26. C. Bluemel, S. Hausmann, P. Fluhr, M. Sriskandarajah, W. B. Stallcup, P. A. Baeuerle, P. Kufer, Epitope distance to the target cell membrane and antigen size determine the potency of T cell-mediated lysis by BiTE antibodies specific for a large melanoma surface antigen. *Cancer Immunol. Immunother.* **59**, 1197–1209 (2010).
27. J. Li, N. J. Stagg, J. Johnston, M. J. Harris, S. A. Menzies, D. DiCara, V. Clark, M. Hristopoulos, R. Cook, D. Slaga, R. Nakamura, L. McCarty, S. Sukumaran, E. Luis, Z. Ye, T. D. Wu, T. Sumiyoshi, D. Danilenko, G. Y. Lee, K. Totpal, D. Ellerman, I. Hötzel, J. R. James, T. T. Junttila, Membrane-proximal epitope facilitates efficient T cell synapse formation by anti-FcRH5/CD3 and is a requirement for myeloma cell killing. *Cancer Cell* **31**, 383–395 (2017).
28. B. Liu, W. Chen, B. D. Evavold, C. Zhu, Accumulation of dynamic catch bonds between TCR and agonist peptide-MHC triggers T cell signaling. *Cell* **157**, 357–368 (2014).
29. S. T. Kim, K. Takeuchi, Z.-Y. Sun, M. Touma, C. E. Castro, A. Fahmy, M. J. Lang, G. Wagner, E. L. Reinherz, The αβ T cell receptor is an anisotropic mechanosensor. *J. Biol. Chem.* **284**, 31028–31037 (2009).
30. M. Bacac, C. Klein, P. Umana, CEA TCB: A novel head-to-tail 2:1 T cell bispecific antibody for treatment of CEA-positive solid tumors. *Oncoimmunology* **5**, e1203498 (2016).
31. D. Slaga, D. Ellerman, T. N. Lombana, R. Vij, J. Li, M. Hristopoulos, R. Clark, J. Johnston, A. Shelton, E. Mai, K. Gadkar, A. A. Lo, J. T. Koerber, K. Totpal, R. Prell, G. Lee, C. Spiess, T. T. Junttila, Avidity-based binding to HER2 results in selective killing of HER2-overexpressing cells by anti-HER2/CD3. *Sci. Transl. Med.* **10**, eaat5775 (2018).
32. G. L. Moore, C. Bautista, E. Pong, D.-H. Nguyen, J. Jacinto, A. Eivazi, U. S. Muchhal, S. Karki, S. Y. Chu, G. A. Lazar, A novel bispecific antibody format enables simultaneous bivalent and monovalent co-engagement of distinct target antigens. *MAbs* **3**, 546–557 (2011).
33. M. Klinger, C. Brandl, G. Zugmaier, Y. Hijazi, R. C. Bargou, M. S. Topp, N. Gökbuget, S. Neumann, M. Goebeler, A. Viardot, M. Stelljes, M. Brüggemann, D. Hoelzer, E. Degenhard, D. Nagorsen, P. A. Baeuerle, A. Wolf, P. Kufer, Immunopharmacologic response of patients with B-lineage acute lymphoblastic leukemia to continuous infusion of T cell–engaging CD19/CD3-bispecific BiTE antibody blinatumomab. *Blood* **119**, 6226–6233 (2012).
34. F. Ravandi, A. S. Stein, H. M. Kantarjian, R. B. Walter, P. Paschka, M. Jongen-Lavrencic, G. J. Ossenkoppele, Z. Yang, B. Mehta, M. Subklewe, A phase 1 first-in-human study of AMG 330, an anti-CD33 bispecific T-cell engager (BiTE®) antibody construct, in relapsed/refractory acute myeloid leukemia (R/R AML). *Blood* **132**, 25 (2018).
35. M. Hutchings, G. Iacoboni, F. Morschhauser, F. Offner, A. Sureda, G. A. Salles, C. Carlo-Stella, J. M. Lopez, D. Thomas, P. N. Morcos, B. Quackenbush, C. Ferlini, M. Bacac, A. M. E. Broeske, N. Dimier, T. Moore, M. Weisser, M. Dickinson, CD20-Tcb (RG6026), a novel "2:1" format T-cell-engaging bispecific antibody, induces complete remissions in relapsed/refractory B-cell Non-Hodgkin's Lymphoma: Preliminary results from a phase I first in human trial. *Blood* **132**, 226 (2018).
36. G. L. Uy, J. Godwin, M. P. Rettig, N. Vey, M. Foster, M. L. Arellano, D. A. Rizzieri, M. S. Topp, G. Huls, B. Lowenberg, G. Martinelli, S. Paolini, F. Ciceri, M. G. Carrabba, C. Ballesteros-Merino, C. B. Bifulco, H. Lelievre, R. La Motte-Mohs, D. Li, J. C. Sun, K. Jacobs, K. Spohn, N. Lonsdale, K. Tran, J. Baughman, M. Shannon, B. Fox, E. Bonvini, J. Wigginton, J. Davidson-Moncada, J. F. DiPersio, Preliminary results of a phase 1 study of flotetuzumab, a CD123 x CD3 Bispecific Dart® Protein, in patients with relapsed/refractory acute myeloid leukemia and myelodysplastic syndrome. *Blood* **130**, 637 (2017).
37. G. R. Chichili, L. Huang, H. Li, S. Burke, L. He, Q. Tang, L. Jin, S. Gorlatov, V. Ciccarone, F. Chen, S. Koenig, M. Shannon, R. Alderson, P. A. Moore, S. Johnson, E. Bonvini, A CD3xCD123 bispecific DART for redirecting host T cells to myelogenous leukemia: Preclinical activity and safety in nonhuman primates. *Sci. Transl. Med.* **7**, 289ra282 (2015).
38. G. Friberg, D. Reese, Blinatumomab (Blincyto): Lessons learned from the bispecific t-cell engager (BiTE) in acute lymphocytic leukemia (ALL). *Ann. Oncol.* **28**, 2009–2012 (2017).

Acknowledgments: We thank M. Ito of Central Institute for Experimental Animals (Kawasaki, Japan) for providing the DKO mice and J. Sampson of Duke University (Durham North Carolina) for providing the huCD3ε-tg mice. We also thank E. de Stanchina for help in developing and passaging the PDX tumors. **Funding:** This work was supported by funds from Enid A. Haupt Endowed Chair (to N.-K.V.C.), the Robert Steel Foundation (to N.-K.V.C.), the Grayer Fellowship (to B.H.S.), and the NIH/NCI Cancer Center Support Grant P30 CA008748. **Author contributions:** B.H.S., M.H., and N.-K.V.C. designed the experiments, interpreted the results, and wrote the manuscript. B.H.S., J.A.P., H.T., and H.-F.G. performed and/or analyzed the experiments. **Competing interests:** B.H.S., M.H., and N.-K.V.C. were named as inventors on U.S. patents filed by MSKCC (Heterodimeric Tetravalency and Specificity Antibody Compositions and Uses Thereof, US 62/774,111). Anti-GD2 antibodies were licensed by MSKCC to Y-mAbs Therapeutics Inc. N.-K.V.C. reports receiving sponsored research grants from Y-mAbs and Abpro-Labs Inc.; holding financial interest in Y-mAbs, Abpro-Labs and Eureka Therapeutics. N.-K.V.C. was also named as an inventor on patents both currently unlicensed and licensed by MSKCC to Y-mAbs Therapeutics, Biotec Pharmacon, or Abpro-Labs [Anti-GD2 Antibodies (h3F8), US 61/397,920; High Affinity Anti-GD2 Antibodies, US 61/801,287; Anti-CD33 Antibody Agents, 62/489,269]. N.-K.V.C. is an advisory board member for Abpro-Labs and Eureka Therapeutics. **Competing interests:** The other authors declare that they have no competing interests. **Data and materials availability:** All data associated with this study are present in the paper or the Supplementary Materials. Antibodies and their amino acid or DNA sequences can be obtained from the corresponding author.

Submitted 24 February 2019
Resubmitted 9 September 2019
Accepted 30 January 2020
Published 11 March 2020
10.1126/scitranslmed.aax1315

Citation: B. H. Santich, J. A. Park, H. Tran, H.-F. Guo, M. Huse, N.-K. V. Cheung, Interdomain spacing and spatial configuration drive the potency of IgG-[L]-scFv T cell bispecific antibodies. *Sci. Transl. Med.* **12**, eaax1315 (2020).

Science Translational Medicine

Interdomain spacing and spatial configuration drive the potency of IgG-[L]-scFv T cell bispecific antibodies

Brian H. Santich, Jeong A. Park, Hoa Tran, Hong-Fen Guo, Morgan Huse and Nai-Kong V. Cheung

Sci Transl Med **12**, eaax1315.
DOI: 10.1126/scitranslmed.aax1315

The specifics of bispecifics

T cell–bispecific antibodies, which are designed to bring T cells together with tumor cells and thereby promote tumor killing, have been attracting increasing attention for a variety of tumor types. These bispecific antibodies come in a variety of shapes, sizes, and configurations, with different studies offering different suggestions as to factors that influence the antibodies' effectiveness. Santich *et al.* undertook a systematic effort to assess the various parameters involved in the antitumor effectiveness of a particular bispecific antibody, examining factors such as valency and spatial configuration, which should help inform the development of future bispecific antibodies.

Science Translational Medicine
AAAS

stm.sciencemag.org/cgi/content/full/12/534/eaax1315/DC1

Supplementary Materials for

Interdomain spacing and spatial configuration drive the potency of IgG-[L]-scFv T cell bispecific antibodies

Brian H. Santich, Jeong A. Park, Hoa Tran, Hong-Fen Guo, Morgan Huse, Nai-Kong V. Cheung*

*Corresponding author. Email: cheungn@mskcc.org

Published 11 March 2020, *Sci. Transl. Med.* **12**, eaax1315 (2020)
DOI: 10.1126/scitranslmed.aax1315

The PDF file includes:

Other Supplementary Material for this manuscript includes the following:

(available at stm.sciencemag.org/cgi/content/full/12/534/eaax1315/DC1)

Data file S1 (Microsoft Excel format). Original data.

SUPPLEMENTARY MATERIALS

Materials and Methods

Protein sequences

Anti-GD2 antibodies (except for GD2.2 and GD2.3) used V_H and V_L domains from hu3F8 (14). Anti-CD3 antibodies used V_H and V_L domains from huOKT3 (15) or 145-2C11 (17). Anti-CD33 antibodies used V_H and V_L domains from huM195 (10). Anti-HER2 control antibodies used V_H and V_L domains from trastuzumab (12). Anti-GPA33 control antibodies used V_H and V_L domains from huA33 (11). IgG-based proteins used a human IgG_1 framework that contained both N297A and K322A mutations to eliminate Fc receptor and complement binding activities, respectively. IgG-[L]-scFv and IgG-[H]-scFv domains used three G_4S_1 domains as a linker between the scFv domain and either C_L or C_{H3} domains, respectively. An additional six G_4S_1 domains were used as a linker between the V_H and V_L domains of the huCD3ε scFv. All control antibodies contained irrelevant tumor-binding domains (anti-CD33, anti-HER2, or anti-GPA33) but retained identical Fc domains and T cell-binding domains (huCD3ε).

Protein production

All proteins were expressed using the Expi293 Expression System (Invitrogen, A14524), according to manufacturer's instructions. Briefly, expression plasmids for each bispecific antibody (BsAb) were amplified and purified using the PureLink HiPure Plasmid Filter Maxiprep Kit (Invitrogen, K210016), then diluted and incubated with Expifectamine (Invitrogen) for 20 minutes before being added to cell suspensions. Cells were incubated in shaker culture for four days or until cell viability dropped <70%, whichever came first. IgG-based proteins were purified with a protein A column using a P920 AKTA FPLC (GE) and eluted with a 1:1 (v/v)

mix of citric acid buffer [43 mM citric acid (Sigma A104), 3 mM sodium citrate (Sigma, S1804)] and sodium citrate solution [25 mM sodium citrate (Sigma), 150 mM sodium chloride (Fisher, S271)]. The BiTE (1+1B) was purified using prepacked Ni^{2+} NTA columns (GE, 11003399) and eluted using 50 mM imidazole (Sigma, 792527). All proteins were buffer exchanged overnight into a pH 8.2 sodium citrate solution [25 mM sodium citrate (Sigma), 150 mM sodium chloride (Fisher)] and subsequently analyzed by SEC-HPLC (Shimadzu) to determine purity.

Heterodimerization

Heterodimerization was achieved using Fab Arm Exchange (FAE), following standard protocols for benchtop scale (*16*). Briefly, K409R or F405L mutations were placed in the Fc regions of each reciprocal pair of IgG or IgG-[L]-scFv BsAbs (tables S1, S5, S7, and S10) to be heterodimerized. Each pair of homodimers was mixed at 1:1 molar ratio and incubated under reducing conditions for five hours at 31 °C. After this incubation, samples were buffer exchanged overnight into a pH 8.2 sodium citrate solution [25 mM sodium citrate (Sigma), 150 mM sodium chloride (Fisher)]. Samples were subsequently moved to 4 °C for another 18-24 hours before being analyzed by SEC-HPLC (Shimadzu) and CZE (Sciex) to assess heterodimerization purity. Sample molecular weight and purity were confirmed by comparing sample chromatograms and peak values to those of known standards (BioRad, 1511901) or parental homodimer samples. The stability of all IgG-based antibodies was evaluated by SEC-HPLC after extended incubations (over three weeks) at 37 °C and 40 °C. No differences in stability were seen with any of the BsAbs.

Cells and cell lines

IMR32 and EL.4 cell lines were obtained from ATCC. IMR32 cells were transfected with luciferase before use in all assays. M14 cell lines were obtained from University of California, Los Angeles, and transfected with luciferase before use in all assays. Nalm6 cell lines were obtained from Dr. Abdel-Wahab at MSKCC and transfected with human CD33 before use in all assays. IMR32, EL.4, M14, and Nalm6 cell lines tested negative for mycoplasma. IMR32, Nalm6, and M14 melanoma cells were validated by STR. All cell lines were maintained in RPMI medium (Corning, 15-040-CM) supplemented with 10% heat inactivated fetal calf serum (VWR, 96068-085), 2 mM L-glutamine (Sigma, G5792), and 1% penicillin/streptomycin (Corning, 30-002-CI). Activated murine T cells (muATCs) were generated by stimulating splenocytes from OT-I Rag2 $^{-/-}$ C57BL/6 transgenic mice. Briefly, OT-I splenocytes were incubated with peptide-pulsed (ovalbumin, SIINFEKL) splenocytes from wild-type C57/BL6 mice in RPMI medium supplemented with 10% heat inactivated fetal calf serum (VWR), 2 mM L-glutamine (Sigma), 1% penicillin/streptomycin (Corning, 30-002-CI), 0.1% 2-mercaptoethanol (Gibco, 21985-023) and 30 U/ml of human IL-2 (aldesleukin, Prometheus Laboratories). T cells were passaged on day 3 after stimulation and supplemented with fresh medium and human IL-2 (aldesleukin) daily. Cells were used for cytotoxicity assays between day 5 and day 8 of culture and were used for flow cytometry assays between day 7 and day 9. Activated human T cells (huATCs) were generated by stimulating healthy donor T cells (consented in protocol NCT02650648) with Human T-Activator CD3/CD28 Dynabeads (Invitrogen, 11131D). Briefly, T cells were incubated with CD3/CD28 beads (bead to T cell ratio of 1:2) in RPMI medium (Corning, 15-040-CM) supplemented with 10% heat inactivated fetal calf serum (VWR), 2 mM L-glutamine (Sigma), 1% penicillin/streptomycin (Corning), and 30 U/ml of human IL-2 (aldesleukin). Cells were passaged on days 2 and 4 and supplemented daily with fresh medium and human IL-2

between day 4 and day 7. T cells were stimulated up to two times (once at day 1 and again at day 8) for up to 21 days of culture. For in vivo experiments, huATCs were used at day 8 of culture (only one stimulation). For in vitro assays (cytotoxicity, cell binding, or conjugate assays), huATCs were used between day 15 and 18 of culture (two stimulations). Patient-derived xenograft (PDX) tumors were established by the antitumor core at MSKCC from surgical samples of patients (consented in protocol NCT00588068).

Cell binding measurements

Cell binding of BsAb was measured by flow cytometry. MuATCs, huATCs, or M14 melanoma cells were incubated with titrations of each BsAb, in duplicate. For staining procedures using IgG-based formats, bound BsAb was detected using an anti-human Fc secondary (Southern Biotech, goat anti-human IgG-PE, 2040-09). For anti-idiotype staining methods, an anti-3F8 or anti-OKT3 idiotype antibody was used for detection. The anti-3F8 idiotype was detected using a goat anti-rat IgG-APC secondary (Biolegend, Clone Poly4054, 405407) and the anti-OKT3 idiotype was detected using a goat anti-mouse IgG-PE (Southern Biotech, 1010-09). Anti-idiotype antibodies were generated at MSKCC and validated by ELISA. All incubations were for 30 minutes at 4 °C. Experiments were repeated multiple times, with graphs presenting a single representative experiment. Samples were acquired using a BD FACSCalibur and analyzed by FlowJo 10.5.3 and GraphPad Prism 8.

Affinity measurements

Binding kinetics were evaluated using SPR (GE, Biacore T200) as described previously (*13*). Briefly, SA or CM5 chips were coated with biotin-GD2 (Elicityl Oligotech) or CD3δε antigens,

respectively (huCD3δε from Acro Biosystems and muCD3δε from Abcam). A five-step titration series of each BsAb was flowed over them, followed by two blank cycles and two regeneration cycles. Binding affinities were calculated using a two-state reaction model with the GE Biacore Evaluation software. Data were plotted using GraphPad Prism 8.

Cytotoxicity measurements

Cytotoxicity was evaluated using a ^{51}Cr release assay. Briefly, target cells were incubated with 100 μCi of sodium chromate (Perkin Elmer) per one million cells for one hour and washed twice. Labeled target cells were then mixed with effector cells (muATC or huATC, 10:1 E:T) and serially titrated BsAb, in triplicate. After four hours, released ^{51}Cr was measured using a gamma counter (Perkins-Elmer). Cell lysis was calculated using the formula [Sample Lysis – Spontaneous lysis]/[Total Lysis – Spontaneous Lysis], where spontaneous lysis measured released ^{51}Cr from target cells without antibody or T cells, and total lysis measured released ^{51}Cr from target cells mixed with 10% SDS. Specific lysis was calculated by subtracting the measured release from a sample without BsAb (T cells and target cells only) from the calculated cell lysis. To calculate the EC_{50}, curves were fitted using a four-parameter logistic fitting with GraphPad Prism 8.

Conjugate formation

huATCs were labeled with CFSE (Invitrogen, C34554), and M14 melanoma cells were labeled with Cell Trace Violet (Invitrogen, C34557). Cells were incubated with 2.5 μM of dye (50 million/ml in PBS) for five minutes at room temperature. The reaction was quenched by the addition of 10-fold excess of complete RPMI and incubated at 37 °C for 20 min. After one wash,

effector and target cells were mixed (1:5 E:T) and added to serially titrated BsAb, in duplicate. After 30 minutes of incubation at 37 °C, cells were fixed (2% PFA) for 10 min (room temperature) and washed once in PBS. Conjugate frequency was calculated as the fraction of T cell:tumor cell conjugates (CTV+/CFSE+) among total T cells (CFSE+), subtracting the average non-specific conjugate rate (T cells + tumor cells without BsAb). Cells were acquired using a BD Fortessa and analyzed using FlowJo 10.5.3. Curves were fitted using a four-parameter logistic fitting with GraphPad Prism 8.

Activation assay

Human peripheral blood mononuclear cells were isolated from leukopacks (New York Blood Center) by ficoll separation. Naïve human T cells were purified using Dynabeads Untouched Human T-cells Kit (Invitrogen, 11344D). Purified T cells were incubated with M14 melanoma cells (10:1 E:T) and serially titrated BsAb, in duplicate. After 20 hours, supernatant was collected and frozen at -80°C for subsequent analysis. Cell pellets were then stained with antibodies against CD4-APC (Biolegend, Clone OKT4, 317416), CD8-PerCP-Cy5.5 (Biolegend, Clone HITα, 300924), CD45-PE-Cy7 (Biolegend, Clone T200, 368532), and CD69-PE (Biolegend, Clone IV A91, 310906) to assess CD69 upregulation. For the 92-hour timepoint, T cells were first labeled with 2.5 μM Cell Trace Violet (Invitrogen), following the conjugate formation protocol. After 92 hours of co-culture, cells were stained with antibodies against CD4-APC (Biolegend, Clone OKT4, 317416), CD8-PerCP-Cy5.5 (Biolegend, Clone HITα, 300924), CD45-PE-Cy7 (Biolegend, Clone T200, 368532), and CD25-PE (Biolegend, Clone BC96, 302606) to assess CD25 upregulation and Cell Trace Violet dilution. Cells were acquired using a

BD Fortessa and analyzed using FlowJo 10.5.3. Curves were fitted using a four-parameter logistic fitting with GraphPad Prism 8.

Cytokine Measurements

Frozen supernatant from the activation assay (20 hour) was used to measure in vitro cytokine production. Human cytokine IL-2 was measured with the 5-plex LEGENDplex Human Th1 Panel (Biolegend, 740723) according to manufacturer guidelines. Frozen plasma samples from the syngeneic animal experiment (4 hours after the first BsAb dose) were used to measure in vivo cytokine production. Mouse cytokine IL-6 was measured with the 5-plex LEGENDplex Mouse Th1 Panel (Biolegend, 740744) according to manufacturer guidelines. Briefly, supernatants were diluted 5-fold and plasma samples were diluted 2-fold, then mixed with appropriate amounts of sample buffer and prelabeled cytokine beads. After two hours of shaking incubation at room temperature, samples were washed and biotinylated secondary antibodies were added. Following a one hour incubation, PE-labeled streptavidin was added directly. After 30 minutes, samples were washed, acquired using a BD FACSCalibur flow cytometer and analyzed using FlowJo 10.5.3. Cytokine concentrations were calculated from a standard curve. Plasma collected separately from non-tumored huCD3ε mice treated with hu3F8 x OKT3 or trastuzumab x OKT3 chemically conjugated BsAb (*21*) were used as positive controls. Curves were fitted using a four-parameter logistic fitting with GraphPad Prism 8.

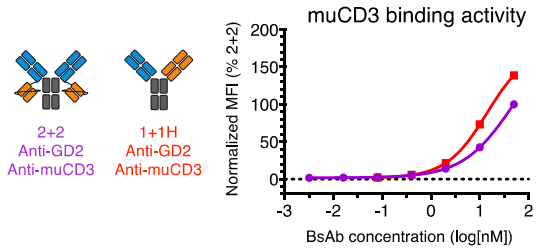

Fig. S1. In vitro binding activity of murine T cell BsAb panel. Schematic of the murine T-cell BsAb panel (left) with representative mouse T cell binding (right), measured by flow cytometry. Geometric mean fluorescence intensity (MFI) was normalized to 2+2 (100%) for each BsAb. For reference: 2+2 is purple, and 1+1H is red. Each curve represents one BsAb, and each point represents a single concentration, with two technical replicates. Data are shown as means ± standard deviation.

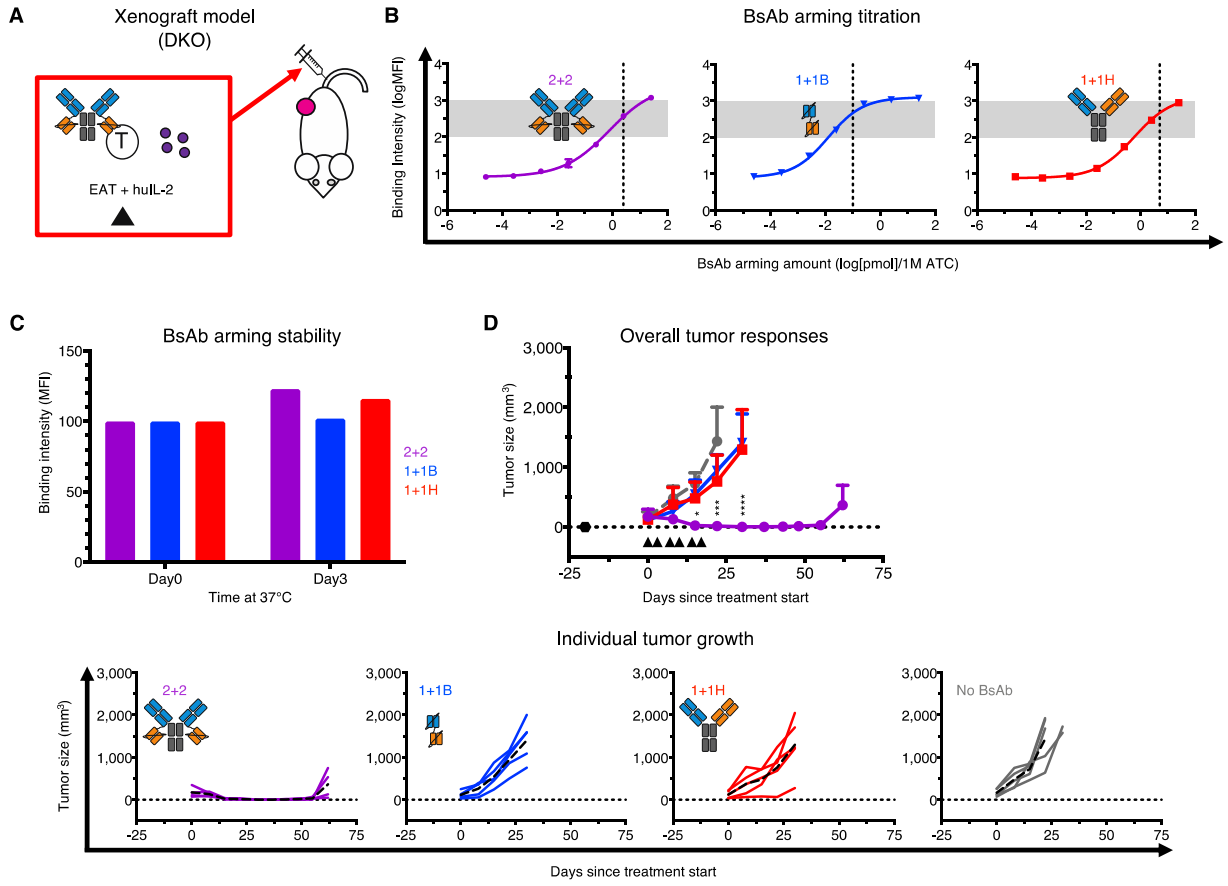

Fig. S2. In vivo tumor responses using EAT xenograft tumor model. (A) Schematics of treatment design for ex vivo "armed" T cell (EAT) xenograft model. EAT were administered intravenously, and human IL-2 (1,000 U) was administered subcutaneously, twice per week (black arrow). For each dose, 20 million huATCs were incubated with 50 pmol of 2+2, 2 pmol of 1+1B, or 100 pmol of 1+1H. (B) Representative titration experiments to determine the arming dose for each BsAb. Each point represents a different concentration of BsAb, with three technical replicates, and the dotted line represents the final concentration used for in vivo experiments. Data are shown as means ± standard deviation. The shaded area represents the target arming concentration (midway between EC_{50} and EC_{Max}). (C) Representative BsAb EAT binding stability. Each bar shows the binding intensity of one BsAb EAT, detected with an anti-GD2 idiotype antibody. Bars are normalized to their initial intensity (day 0). (D) Average (top)

and individual mouse (bottom) tumor responses in each group. In the overall response graph, each line represents one treatment group (n=5). The dotted black line represents no measurable tumor, and the black hexagon represents the tumor implantation. Tumor averages were calculated until at least one mouse had to be euthanized. Data are shown as means ± standard deviation. In the individual response graphs, each line represents a single mouse, and the dashed line represents the group average. For reference: 2+2 is purple, 1+1B is blue, 1+1H is red, and unarmed huATC (No BsAb) is gray. In this experiment, the lot of 1+1B used was 85% pure by SEC-HPLC but showed identical activity to the lot used in vitro. Statistical significances were calculated by two-way analysis of variance (ANOVA) and Tukey correction. *$P < 0.05$, ***$P < 0.0002$ for control, 1+1B, or 1+1H compared to 2+2. ****$P < 0.0001$ for 1+1B or 1+1H compared to 2+2.

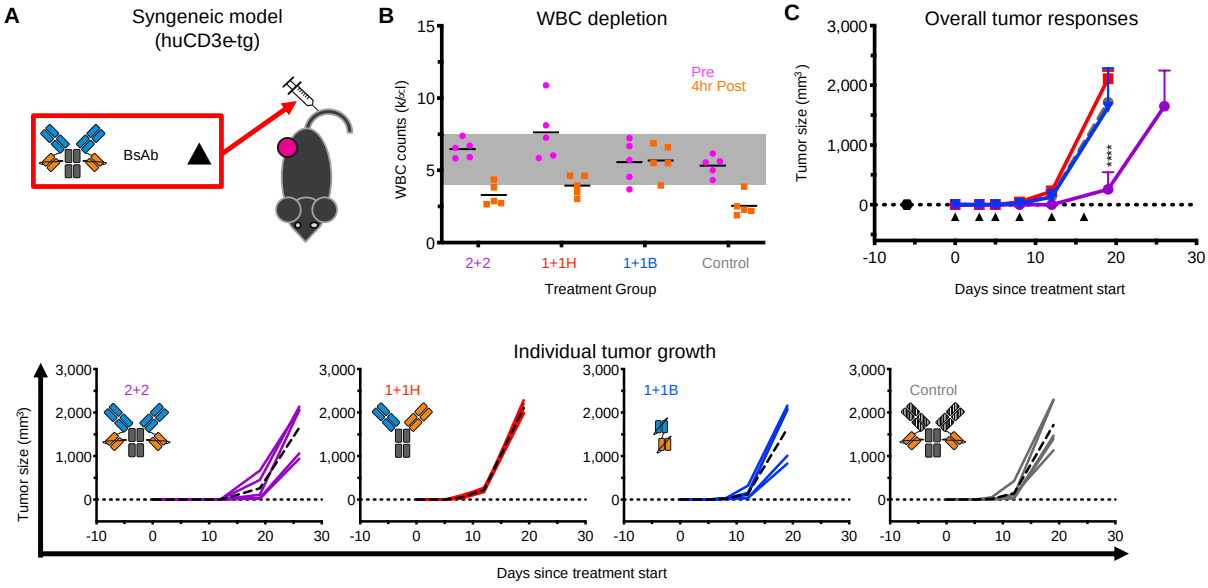

Fig. S3. In vivo tumor responses using syngeneic tumor model. (A) Schematic of the treatment design for the syngeneic tumor model. 25 pmol of BsAb was administered intravenously twice per week (black triangle). An anti-HER2 BsAb was used as a control. (B) White blood cell (WBC) counts before (purple) and four hours after (orange) the first BsAb dose. The gray bar represents the mean ± one standard deviation of WBC counts from non-tumored age-matched mice (n=15). (C) Average (top) and individual mouse (bottom) tumor responses in each group. In the overall response graph, each line represents one treatment group (n=5). The dotted black line represents no measurable tumor, and the black hexagon represents the tumor implantation. Tumor averages were calculated until at least one mouse had to be euthanized. Data are shown as means ± standard deviation. In the individual response graphs, each line represents a single mouse, and the dashed line represents the group average. For reference: 2+2 is purple, 1+1B is blue, 1+1H is red, and the control BsAb is gray. In this experiment, the lot of 1+1B used was 85% pure by SEC-HPLC but showed identical activity to the lot used in vitro. Statistical significances were calculated by two-way analysis of variance (ANOVA) and Tukey correction. ****P < 0.0001 for control, 1+1B, or 1+1H compared to 2+2.

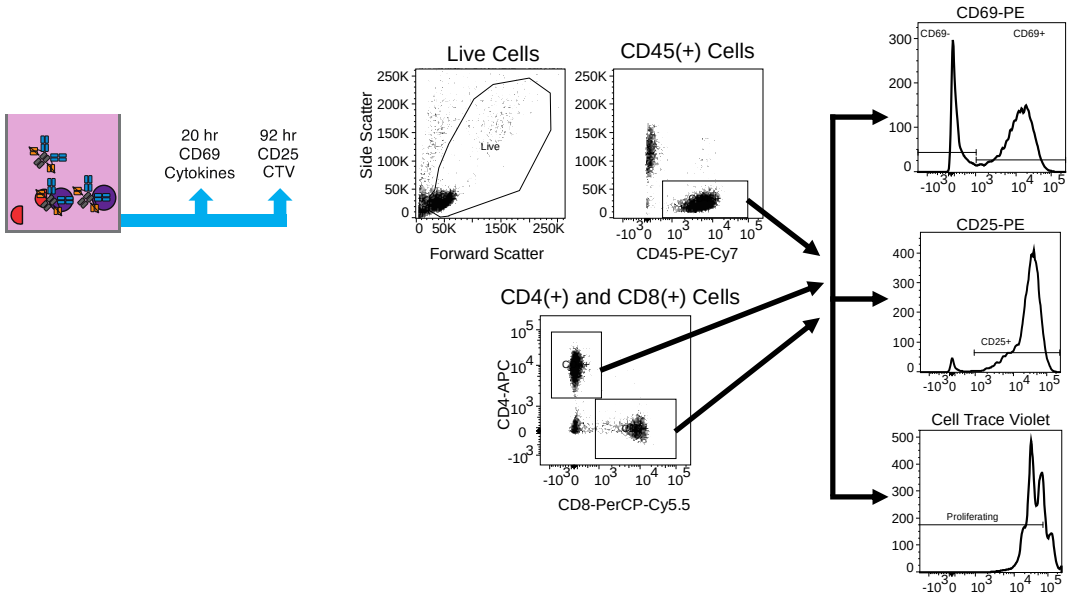

Fig. S4. In vitro coculture assay analysis. Schematic of flow cytometry analysis from representative sample, using Flowjo. Live cells were gated, followed by CD45(+) cells to exclude any remaining tumor cells. Cells were then analyzed for CD69 or CD25 expression or CTV dilution. CD4(+) and CD8(+) T cell subsets were also gated on and analyzed separately.

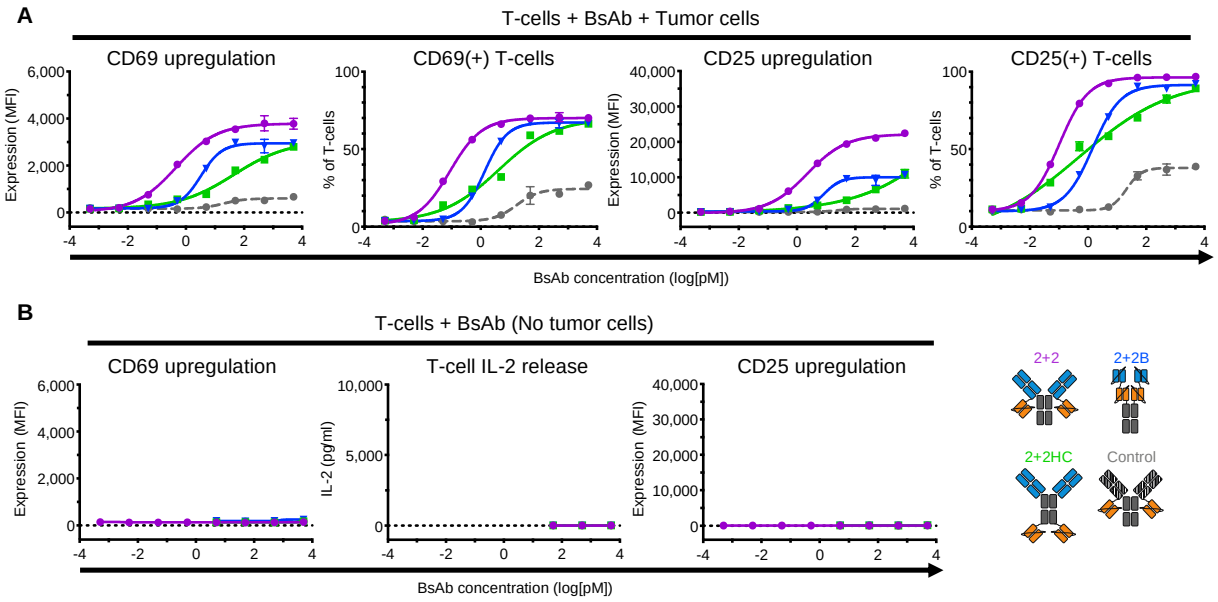

Fig. S5. Naïve T cell activation by dual bivalent BsAb formats. (A) T cell activation after co-culture with BsAb in the presence of tumor. CD69 (left) and CD25 (right) expression and frequency of expression on T cells. (B) T cell activation after co-culture with BsAb in the absence of tumor. CD69 expression (left) and IL-2 release (middle) after 20-hour incubations. CD25 expression (right) after 92-hour incubation. Each line represents a single BsAb, and each point represents a single concentration, with two technical replicates. Schematics (bottom right) for reference: 2+2 is purple, 2+2B is blue, 2+2HC is green, and the control BsAb is gray. Data are shown as means ± standard deviation.

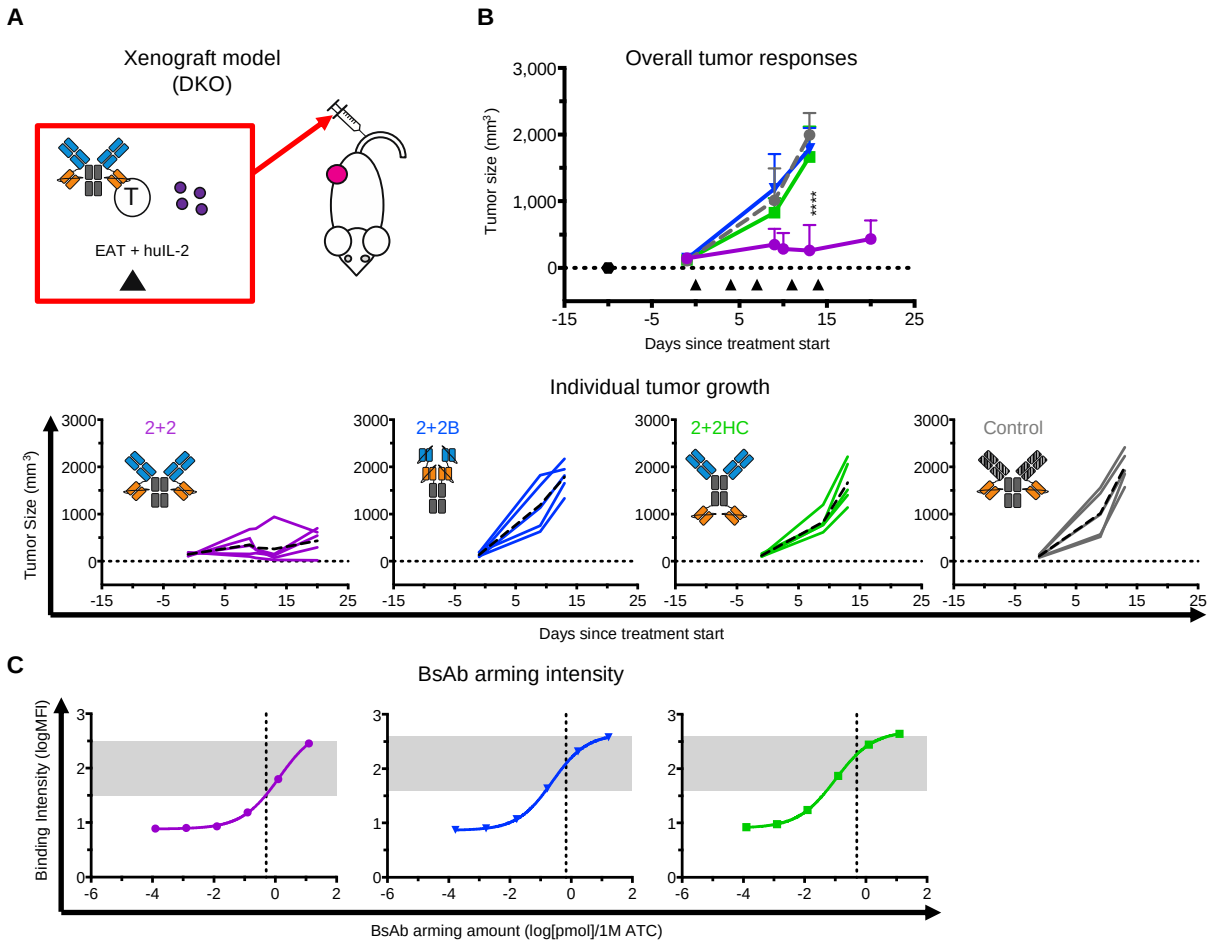

Fig. S6. In vivo tumor responses using EAT xenograft tumor model. (A) Schematics of treatment design for ex vivo "armed" T cell (EAT) xenograft model. EATs were administered intravenously, and human IL-2 (1,000 U) was administered subcutaneously, twice per week (black arrow). For each dose, 20 million huATCs were armed with 10 pmol of IgG-[L]-scFv, 13 pmol of BiTE-Fc, and 10 pmol of IgG-[H]-scFv. (B) Average (top) and individual mouse (bottom) tumor responses in each group. In the overall response graph, each line represents one treatment group (n=5). The dotted black line represents no measurable tumor, and the black hexagon represents the tumor implantation. Tumor averages were calculated until at least one mouse had to be euthanized. Data are shown as means ± standard deviation. In the individual response graphs, each line represents a single mouse, and the dashed line represents the group

average. (C) Representative titration experiments to determine the arming dose for each BsAb. Each point represents a different concentration of BsAb, with three technical replicates, and the dotted line represents the final concentration used for in vivo experiments. Data are shown as means ± standard deviation. The shaded area represents the target arming concentration (midway between EC_{50} and EC_{Max}). For reference: 2+2 is purple, 2+2B is blue, 2+2HC is green, and the control BsAb is gray. Statistical significances were calculated by two-way analysis of variance (ANOVA) and Tukey correction. ****$P < 0.0001$ for control, 2+2B, or 2+2HC compared to 2+2.

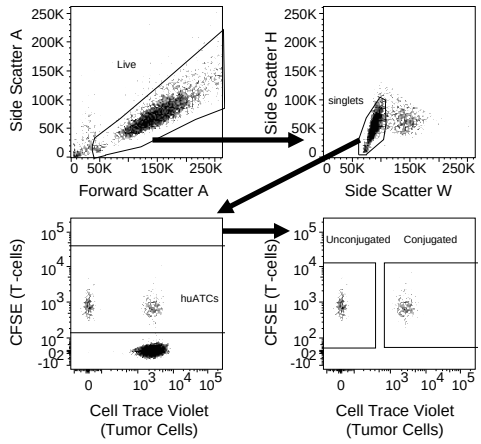

Fig. S7. In vitro conjugate assay analysis. Schematic of in vitro conjugate assay analysis using human T cells and M14 melanoma cells. Live cells were gated, followed by singlet gating. All CFSE-expressing T cells were then gated to separate unconjugated target cells. T cells were then gated based on co-expression of cell trace violet (on tumor cells) indicating that they are conjugated to tumor cells.

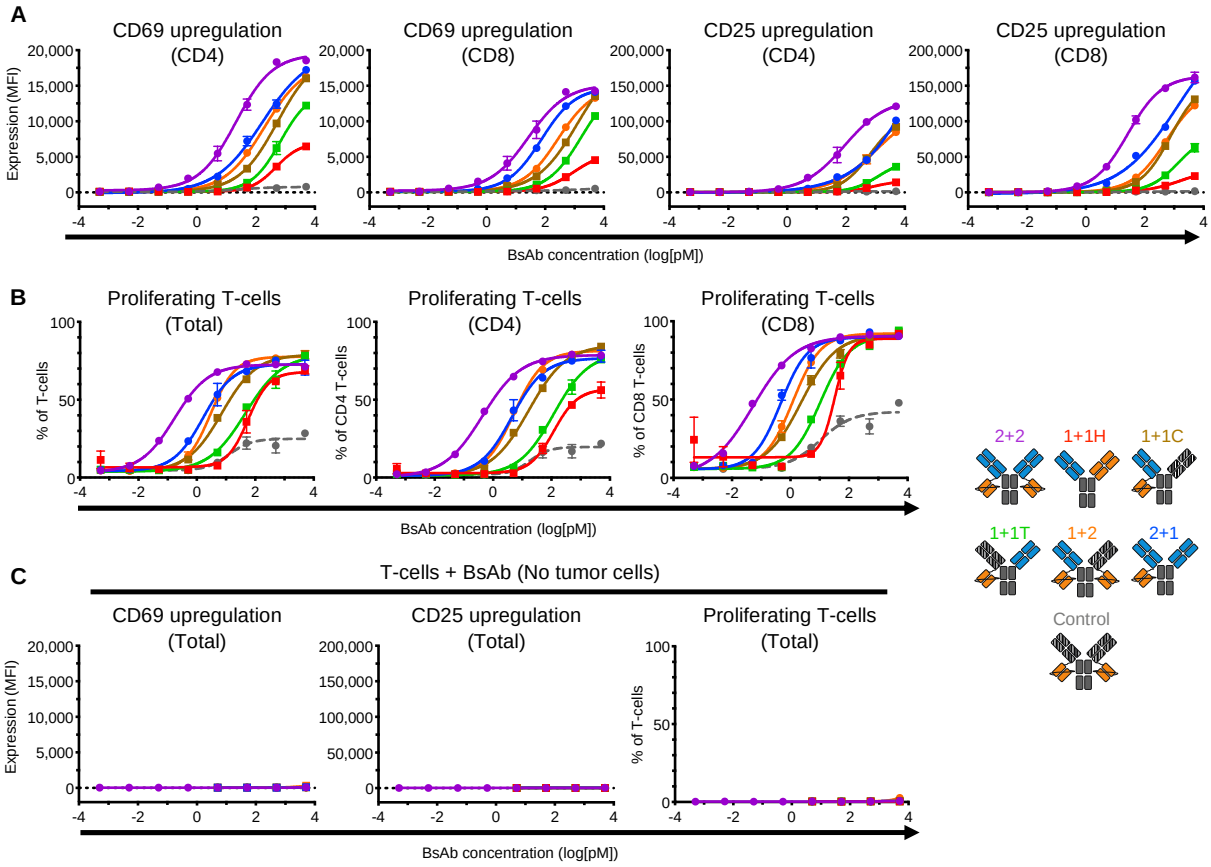

Fig. S8. T cell activation using the IgG-[L]-scFv panel. (A-B) T cell activation and proliferation after co-culture with BsAb in the presence of tumor. (A) CD69 (left) and CD25 (right) expression on CD4 and CD8 T cells. (B) Total (left), CD4 (center), and CD8 (right) T cell proliferation after co-culture. (C) T cell activation (left, center) or proliferation (right) after incubation with BsAb in the absence of tumor. Schematics (right) for reference: 2+2 is purple, 1+1H is red, 2+1 is blue, 1+1T is green, 1+1C is brown , 1+2 is orange, and the control the BsAb is gray. Each line represents a single BsAb, and each point represents a single concentration, with two technical replicates. Data are shown as means ± standard deviation.

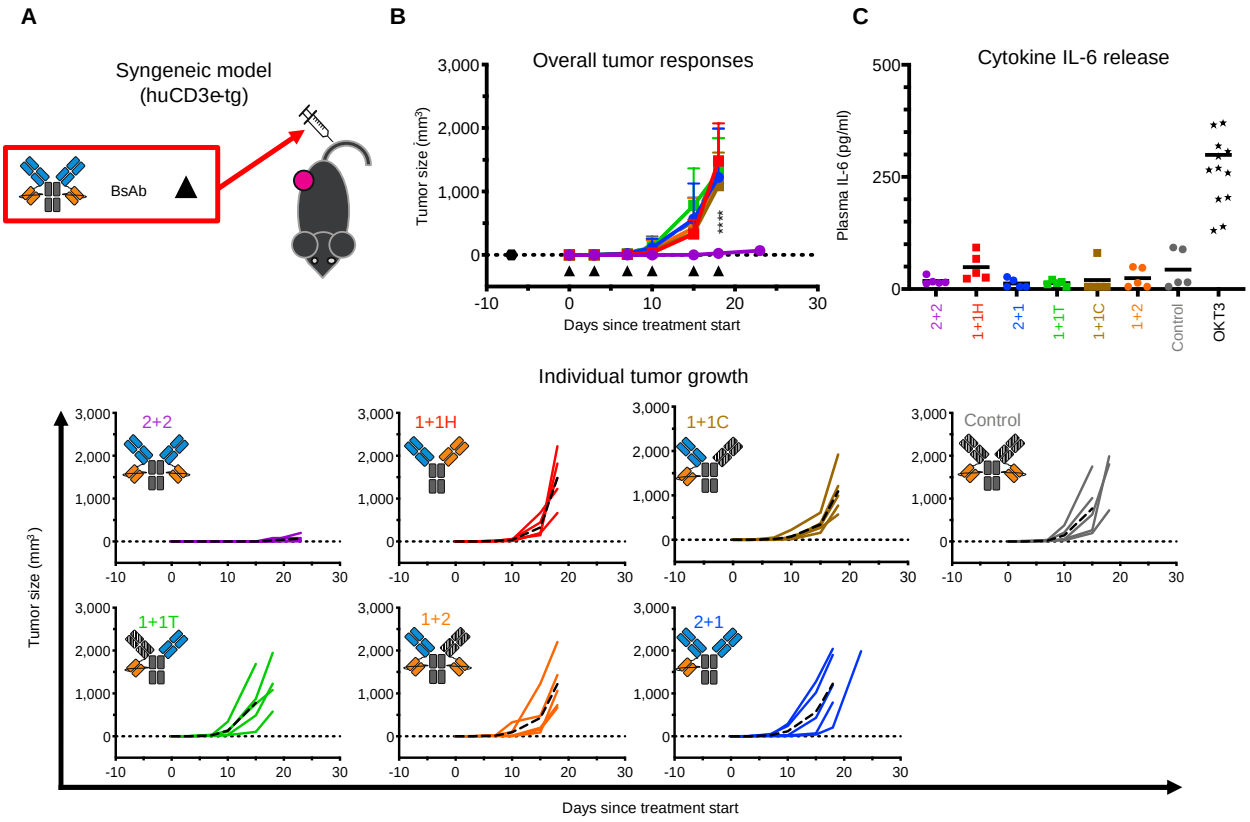

Fig. S9. In vivo tumor responses using syngeneic tumor model. (A) Schematic of the treatment design for the syngeneic tumor model. 25 pmol of BsAb was administered intravenously twice per week (black triangle). An anti-CD33 BsAb was used as a control. (B) Average (top) and individual mouse (bottom) tumor responses in each group. In the overall response graph, each line represents one treatment group (n=5). The dotted black line represents no measurable tumor, and the black hexagon represents the tumor implantation. Tumor averages were calculated until at least one mouse had to be euthanized. Data are shown as means ± standard deviation. In the individual response graphs, each line represents a single mouse, and the dashed line represents the group average. (C) Plasma IL-6 concentrations four hours after the first BsAb dose. Each point represents a single mouse. The positive control is a chemically conjugated BsAb containing OKT3 IgG. For reference: 2+2 is purple, 1+1H is red, 2+1 is blue, 1+1T is green, 1+1C is brown, 1+2 is orange, and the control the BsAb is gray. Statistical

significances were calculated by two-way analysis of variance (ANOVA) and Tukey correction.

****$P < 0.0001$ for control, 2+1, 1+2, 1+1C, 1+1T, or 1+1H compared to 2+2.

Table S1. In vitro properties and design of anti-GD2 BsAb.

BsAb	EC_{50} (pM)	Fold Change	GD2 Valency	CD3 Valency	K409R mAb	F405L mAb	SEC-HPLC Purity (%)
2+2	0.009	-	2	2	-	-	96%
1+1B	0.234	26	1	1	-	-	99%
1+1H	4.475	497	1	1	IgG(hu3F8)	IgG(huOKT3)	98%

Summary of in vitro cytotoxicity EC_{50}, fold-difference in EC_{50}, antigen valency, FAE design, and protein purity by SEC-HPLC for common BsAb panel. Fold change is calculated in reference to the EC_{50} of 2+2. Purity is calculated as the fraction of protein at correct elution time out of the total protein by area under the curve of the SEC-HPLC chromatogram.

Table S2. GD2 binding kinetics for BsAb using SPR.

BsAb	Apparent K_D (nM)	Fold Change	k_{a1} (1/Ms)	k_{d1} (1/s)	k_{a2} (1/s)	k_{d2} (1/s)	Chi^2 (RU^2)
2+2	2.5	-	1.0E+06	1.1E-02	1.9E-02	5.6E-03	2.6
1+1B	11	5	2.2E+05	8.3E-02	2.5E-02	7.8E-04	79.9
1+1H	15	6	2.2E+05	5.8E-02	3.0E-02	1.8E-03	2.7

GD2 binding kinetics summary for common BsAb panel. Data were generated from two-state reaction model using Biacore Evaluation software. Chi^2 represents deviation of the fitted data from the experimental data measured in RU. Fold change is calculated in reference to the K_D of 2+2.

Table S3. huCD3ε binding kinetics for BsAb using SPR.

BsAb	Apparent K_D (nM)	Fold Change	k_{a1} (1/Ms)	k_{d1} (1/s)	k_{a2} (1/s)	k_{d2} (1/s)	Chi^2 (RU^2)
2+2	5.8	-	4.1E+06	2.0E-01	9.5E-03	1.3E-03	9.7
1+1B	13	2	9.2E+07	2.5E+00	5.7E-03	5.6E-03	1.8
1+1H	130	22	9.4E+05	1.2E+00	2.5E-02	2.7E-03	0.9

huCD3ε binding kinetics summary for common BsAb panel. Data were generated from two-state reaction model using Biacore Evaluation software. Chi^2 represents deviation of the fitted data from the experimental data measured in RU. Fold change is calculated in reference to the K_D of 2+2.

Table S4. In vitro properties and design of additional anti-GD2 BsAb.

BsAb	EC_{50} (pM)	Fold Change	GD2 Valency	CD3 Valency	K409R mAb	F405L mAb	SEC-HPLC Purity (%)
GD2.2 2+2	0.024	-	2	2	-	-	98%
GD2.2 1+1H	21	875	1	1	IgG(GD2.2)	IgG(huOKT3)	96%
GD2.2 1+1B	3.31	138	1	1	-	-	98%
GD2.3 2+2	0.049	-	2	2	-	-	98%
GD2.3 1+1H	96	1959	1	1	IgG(GD2.3)	IgG(huOKT3)	100%
2C11 2+2	0.804	-	2	2	-	-	96%
2C11 1+1H	9.869	12.3	1	1	IgG(hu3F8)	IgG(ch2C11)	96%

Summary of in vitro cytotoxicity EC_{50}, fold-difference in EC_{50}, antigen valency, FAE design, and protein purity by SEC-HPLC for additional anti-GD2 BsAb panel. Fold change is calculated in reference to the EC_{50} of matching 2+2. Purity is calculated as the fraction of protein at correct elution time out of the total protein by area under the curve of the SEC-HPLC chromatogram.

Table S5. muCD3ε binding kinetics for BsAb using SPR.

BsAb	Apparent K_D (nM)	Fold Change	k_a (1/Ms)	k_d (1/s)	Chi^2 (RU^2)
2C11 2+2	61.5	-	2.5E+04	1.5E-03	0.03
2C11 1+1H	94.6	1.5	6.0E+04	5.7E-03	0.15

muCD3ε binding kinetics summary for the 2C11 BsAb panel. Data were generated from 1:1 fitting using Biacore Evaluation software. Chi^2 represents deviation of the fitted data from the experimental data measured in RU. Fold change is calculated in reference to the K_D of 2C11 2+2.

Table S6. In vivo pharmacokinetics of 2+2 BsAb.

	$T_{1/2}$ (d)	C_{max} (mg/mL)	C_{min} (mg/mL)	AUC (0-168h) (h*mg/mL)	AUC (0-∞) (h*mg/mL)	Cl_{obs} (mL/h)	Cl_{pred} (mL/h)	Vss_{obs} (mL)	Vss_{pred} (mL)
2+2	3.68	36.58	3.23	1269.40	1680.61	0.060	0.061	6.65	6.55
IgG	3.51	25.67	2.09	948.95	1203.02	0.083	0.083	8.53	8.52

Summary of pharmacokinetic data for 2+2 and hu3F8 IgG (for reference). Mice (n=5) were injected with 100 μg of each protein, and blood samples were drawn retroorbitally serially over 7 days. Samples were processed to collect serum and frozen until analysis. Pharmacokinetic analysis was carried out by non-compartmental analysis of the serum concentration-time data using WinNonlin software program (Pharsight Corp.).

Table S7. In vitro properties and design of dual bivalent BsAb.

BsAb	EC_{50} (pM)	Fold Change	GD2 Valency	CD3 Valency	SEC-HPLC Purity (%)
2+2	0.038	-	2	2	96%
2+2B	0.133	3	2	2	93%
2+2HC	0.080	2	2	2	98%

Summary of in vitro cytotoxicity EC_{50}, fold-difference in EC_{50}, antigen valency, and protein purity of the dual bivalent BsAb panel. Fold change is calculated in reference to the EC_{50} of 2+2. Purity is calculated as the fraction of protein at correct elution time out of the total protein by area under the curve of the SEC-HPLC chromatogram.

Table S8. In vitro properties and design of anti-GD2 IgG-[L]-scFv panel.

BsAb	EC_{50} (pM)	Fold Change	GD2 Valency	CD3 Valency	K409R mAb	F405L mAb	SEC-HPLC Purity (%)	CZE Purity (%)
2+2	0.026		2	2	-	-	96%	-
1+1H	20	748	1	1	IgG(hu3F8)	IgG(huOKT3)	98%	95%
2+1	0.240	9	2	1	IgG(hu3F8)	IgG(hu3F8)-[L]-scFv(huOKT3)	95%	97%
1+2	0.773	29	1	2	IgG(huM195)-[L]-scFv(huOKT3)	IgG(hu3F8)-[L]-scFv(huOKT3)	92%	95%
1+1C	0.784	30	1	1	IgG(huM195)	IgG(hu3F8)-[L]-scFv(huOKT3)	94%	94%
1+1T	37	1404	1	1	IgG(hu3F8)	IgG(huM195)-[L]-scFv(huOKT3)	94%	94%

Summary of in vitro cytotoxicity EC_{50}, fold-difference in EC_{50}, antigen valency, FAE design, and protein purity of the anti-GD2 IgG-[L]-scFv panel. Fold change is calculated in reference to the EC_{50} of 2+2. Purity is calculated as the fraction of protein at correct elution time out of the total protein by area under the curve of the SEC-HPLC chromatogram or by area under the curve of the CZE chromatogram.

Table S9. GD2 binding kinetics for IgG-[L]-scFv panel using SPR.

BsAb	Apparent K_D (nM)	Fold Change	k_{a1} (1/Ms)	k_{d1} (1/s)	k_{a2} (1/s)	k_{d2} (1/s)	Chi^2 (RU^2)
2+2	2.8	-	6.2E+05	6.2E-03	2.3E-02	8.9E-03	0.1
1+1H	31	11	1.7E+05	6.9E-02	2.2E-02	1.8E-03	7.6
2+1	2.5	1	7.4E+05	7.0E-03	2.7E-02	9.9E-03	0.1
1+2	31	11	1.1E+05	9.8E-02	2.8E-02	9.7E-04	4.4
1+1C	30	11	9.8E+04	1.1E-01	2.7E-02	7.7E-04	1.1
1+1T	27	10	1.3E+05	1.0E-01	2.8E-02	9.6E-04	1.8

GD2 binding kinetics summary for heterodimeric IgG-[L]-scFv panel. Data were generated from two-state reaction model using Biacore Evaluation software. Chi^2 represents deviation of the fitted data from the experimental data measured in RU. Fold change is calculated in reference to the K_D of 2+2.

Table S10. huCD3ε binding kinetics for IgG-[L]-scFv panel using SPR.

BsAb	Apparent K_D (nM)	Fold Change	k_{a1} (1/Ms)	k_{d1} (1/s)	k_{a2} (1/s)	k_{d2} (1/s)	Chi^2 (RU^2)
2+2	10	-	9.7E+06	3.1E-01	4.2E-03	2.0E-03	8.5
1+1H	70	7	3.6E+05	3.6E-01	3.4E-02	2.6E-03	2.1
2+1	310	30	1.5E+05	1.4E-01	9.8E-03	5.2E-03	0.7
1+2	11	1	3.2E+06	2.2E-01	7.5E-03	1.4E-03	4.9
1+1C	110	11	1.5E+05	6.6E-02	1.0E-02	3.5E-03	0.5
1+1T	94	9	1.0E+05	1.0E-01	2.2E-02	2.3E-03	0.5

huCD3ε binding kinetics summary for heterodimeric IgG-[L]-scFv panel. Data were generated from two-state reaction model using Biacore Evaluation software. Chi^2 represents deviation of the fitted data from the experimental data measured in RU. Fold change is calculated in reference to the K_D of 2+2.

Table S11. In vitro properties and design of anti-CD33 IgG-[L]-scFv panel.

BsAb	EC_{50} (pM)	Fold Change	CD33 Valency	CD3 Valency	K409R mAb	F405L mAb	SEC-HPLC Purity (%)	In GD2 panel*
CD33 2+2	0.9		2	2	-	-	92%	No
CD33 1+1H	134.4	149	1	1	IgG(huM195)	IgG(huOKT3)	94%	No
CD33 2+1	4.5	5	2	1	IgG(huM195)	IgG(huM195)-[L]-scFv(huOKT3)	97%	No
1+2*	6.0	6.7	1	2	IgG(huM195)-[L]-scFv(huOKT3)	IgG(hu3F8)-[L]-scFv(huOKT3)	92%	Same as GD2 1+2
CD33 1+1T*	500	555	1	1	IgG(huM195)	IgG(hu3F8)-[L]-scFv(huOKT3)	94%	Same as GD2 1+1C
CD33 1+1C*	11.5	12.3	1	1	IgG(hu3F8)	IgG(huM195)-[L]-scFv(huOKT3)	94%	Same as GD2 1+1T

Summary of in vitro cytotoxicity EC_{50}, fold-difference in EC_{50}, antigen valency, FAE design, and protein purity of the anti-CD33 IgG-[L]-scFv panel. Fold change is based on the EC_{50} of 2+2. Purity is calculated as the fraction of protein at correct elution time out of the total protein by area under the curve of the SEC-HPLC chromatogram.